Tectonophysics 665 (2015) 1–16

Contents lists available at ScienceDirect

Tectonophysics

journal homepage: www.elsevier.com/locate/tecto

Transition from orogen-perpendicular to orogen-parallel exhumation and cooling during crustal indentation — Key constraints from $^{147}Sm/^{144}Nd$ and $^{87}Rb/^{87}Sr$ geochronology (Tauern Window, Alps)

Silvia Favaro [a,*], Ralf Schuster [b], Mark R. Handy [a], Andreas Scharf [a,1], Gerhard Pestal [b]

[a] Department of Earth Sciences, Freie Universität Berlin, Malteserstrasse 74-100, 12249 Berlin, Germany
[b] Geologische Bundesanstalt, Neulinggasse 38, 1030 Wien, Austria

ARTICLE INFO

Article history:
Received 9 March 2015
Received in revised form 18 August 2015
Accepted 23 August 2015
Available online 12 September 2015

Keywords:
Doming
Indentation
Exhumation
Lateral escape
Cooling
Tauern Window

ABSTRACT

The core of the Alpine orogen in the Eastern Alps (Tauern Window) experienced a change from orogen-normal shortening and post-nappe doming to predominantly orogen-parallel extension and tectonic unroofing during late Oligocene to Miocene northward indentation of the Adriatic Microplate. A new $^{147}Sm/^{144}Nd$ isochron age of 25.7 ± 0.9 Ma on a garnet-bearing assemblage from the lowest nappe complex forming a dome in the eastern part of the Tauern Window indicates that high temperatures related to post-nappe Barrovian-type metamorphism overlapped in time with the onset of doming. New $^{87}Rb/^{87}Sr$ biotite ages from this same complex combined with previously published $^{87}Rb/^{87}Sr$ white mica ages suggest that doming and exhumation began no later than 28 Ma immediately in front of indenting Austroalpine crustal blocks, then migrated laterally to the ESE during rapid exhumation and orogen-parallel stretching beginning at about 23 Ma. Rapid cooling ended at approximately 17 Ma in the footwall of the Katschberg Normal Fault, which delimits the eastern margin of the Tauern Window. A similar pattern of migrating doming, orogen-parallel extension and cooling is recognized in the western part of the Tauern Window, where rapid exhumation began at about 20 Ma, some 2–3 Ma later than in the eastern part. This difference in the onset of rapid exhumation as well as the overall migration of doming from the center to the ends of the Tauern Window are attributed to fragmentation of the aforementioned Austroalpine blocks along the leading edge of the main Adriatic indenter (Southern Alps) as this indenter advanced to the north.

1. Introduction

Orogenic crust responds to indentation by a combination of crustal thickening, erosion and orogen-parallel extension leading to lateral orogenic escape (Royden and Burchfield, 1989; Ratschbacher et al., 1989, 1991b; Selverstone, 2005). The response to indentation is influenced by several factors including the shape and rigidity of the indenter as well as the thermo-mechanical state of the orogenic crust (e.g., Tapponnier et al., 1986; Rosenberg et al., 2007; Luth et al., 2013).

The Tauern Window in the Eastern Alps (Fig. 1) is an excellent place to study indentation processes because it reveals an almost complete stratigraphic and tectonic record of the transition from collision to indentation. It contains part of the Alpine orogenic wedge with thrust slices of European continental crust (Subpenninic nappes) and Alpine Tethyan oceanic units (Penninic nappes) accreted to overlying Austroalpine units derived from the margin of the Adriatic microplate (e.g., Kober, 1920; Staub, 1924; Exner, 1971, 1982; Tollmann, 1977; Thiele, 1980; Kurz et al., 1996, 1998; Schmid et al., 2013). The Tauern Window formed when the leading edge of this microplate pushed northward into the Alpine orogenic wedge (Fig. 1, Ratschbacher et al., 1991b; Scharf et al., 2013a; Schmid et al., 2013). Two amphibolite-facies metamorphic domes, the Eastern and Western Tauern Domes (ETD and WTD in Fig. 1), exhumed the deepest nappes of highly metamorphosed European continental crust (Venediger Nappe System). These domes are delimited by low-angle normal faults, the Brenner and Katschberg Normal Faults (BNF, KNF in Fig. 1) that accommodated orogen-parallel stretching in Miocene time (e.g., Behrmann, 1988; Selverstone, 1988; Genser and Neubauer, 1989; Scharf et al., 2013a; Schneider et al., submitted for publication). Both the ETD and WTD show concentric Oligo–Miocene cooling age patterns for the $^{87}Rb/^{87}Sr$ white mica (500 °C) and biotite (300 °C) systems, but the ages in the WTD are younger than in the ETD by some 2–3 Ma (Fügenschuh et al., 1997; Frisch et al., 1998, 2000; Linzer et al., 2002; Handy et al., 2005; Luth and Willingshofer, 2008; Scharf et al., 2013a; Scharf et al., submitted for publication). Existing studies show that the cooling history may be heterogeneous even on the scale of the domes themselves (Reddy et al., 1993); in the ETD, $^{87}Rb/^{87}Sr$ white mica and biotite ages in the

* Corresponding author. Tel.: +49 3 838 70190.
E-mail address: silvia.favaro@fu-berlin.de (S. Favaro).
[1] Now at Department of Earth Science, Sultan Qaboos University, P.O. Box 36, Al-Khoudh, P.C. 123, Muscat, Sultanate of Oman.

http://dx.doi.org/10.1016/j.tecto.2015.08.037
0040-1951/

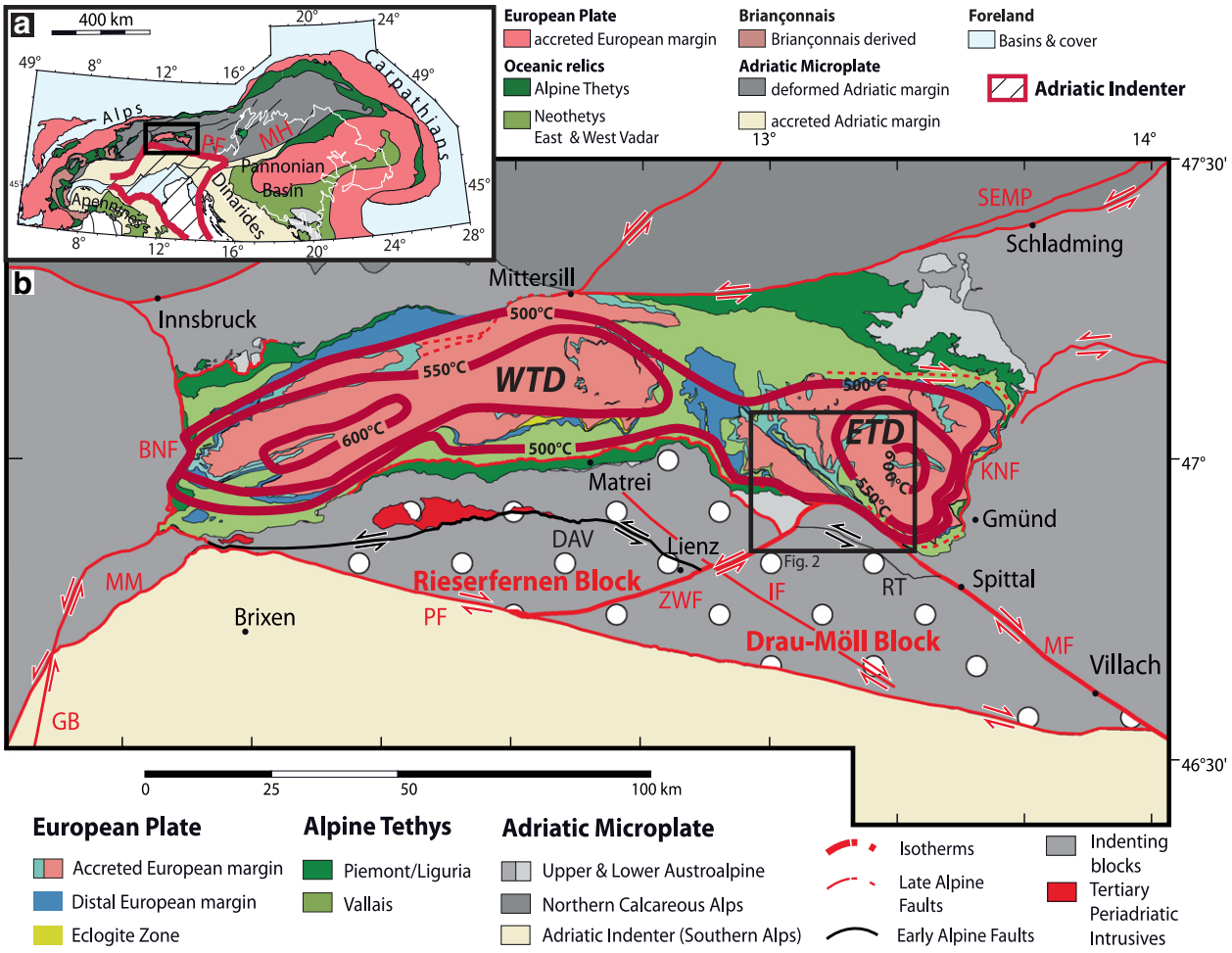

Fig. 1. (a) Tectonic overview of the Alps and the Carpathians (modified from Schmid et al., 2008); (b) tectonic map of the Tauern Window: WTD and ETD — Western and Eastern Tauern domes with isotherms for peak of Barrovian metamorphism. Major faults relevant to this study: BNF — Brenner Normal Fault; DAV — Defereggen–Antholz–Vals Fault; GB — Giudicarie Belt including sinistral strike-slip faults; IS — Iseltal Fault; KNF — Katschberg Normal Fault; MF — Mölltal Fault; MH — Mid-Hungarian Fault; MM — Meran–Mauls Fault; PF — Periadriatic Fault; RT — Ragga–Teuchl Fault, SEMP — Salzach–Ennstal–Mariazell–Puchberg Fault; ZWF — Zwischenbergen–Wöllatratten. Map modified from Schmid et al. (2013) with isotherms for 500° and 550 °C in the western and central parts of the Tauern Window taken from the compilation of Bousquet et al. (2012) and in the ETD from Scharf et al. (2013b), Droop (1985, 2013) and own data.

northwestern part are some 5 Ma older than in the southeastern part (Cliff et al., 1985).

Interpreting the cooling history of deeply buried rocks in terms of exhumation is tricky because rocks are poor heat conductors and their rise to the surface in active orogens is usually faster than their ability to thermally equilibrate (e.g., England and Thompson, 1984). If it is presumed that the heterogeneous cooling of the ETD obtained from existing radiometric ages is real, then this cooling can be interpreted either to indicate coeval exhumation at different exhumation rates (i.e., slower in the northwestern than in the southeastern part of the ETD) and/or diachronous exhumation that migrated from northwest to southeast across the ETD. This dilemma bears obvious implications for the response of the orogenic crust to indentation and lateral escape; in the former case, exhumation was immediate but non-uniform, whereas in the latter, exhumation migrated away from the indenting Austroalpine blocks, affecting successively more external parts of the Alpine wedge. Testing these hypotheses is one of the main goals of this paper.

The duration of orogen-parallel stretching along the Katschberg Normal Fault, as well as the effect of the indenter shape on the cooling and exhumation pattern remain enigmatic; in particular, the timing of the onset of doming and normal faulting is not yet well constrained. Previous work has suggested that rapid exhumation in the Tauern Window may have been diachronous, with ETD beginning to exhume already before the onset of rapid exhumation in the WTD at 20 Ma and prior to northward motion of the Southern Alps indenter along the Giudicarie Belt beginning at 21–23 Ma (Scharf et al., 2013a). This belt comprises both oblique thrusts and a sinistral strike-slip fault that offsets the Periadriatic Fault (Fig. 1; e.g., Pomella et al., 2012). Dating of structurally key minerals with isotopic closure temperatures in the 300–500 °C range potentially enables us to determine the onset of rapid cooling and, therefore, place time limits on the beginning of rapid exhumation.

This paper integrates new $^{87}Rb/^{87}Sr$ and $^{147}Sm/^{144}Nd$ ages with microstructural studies of key mineral assemblages (garnet, white mica and biotite) to date the onset of tectonic unroofing and to show how exhumation and cooling migrated within the ETD. By relating new and existing ages to the first-order structures of indentation, a new model is proposed in which orogen-normal exhumation was transitional to orogen-parallel exhumation during fragmentation and faulting of the leading edge of the advancing Adriatic indenter. Finally, rapid cooling of the European orogenic crust in the ETD is discussed in the broader context of the evolution of the Tauern Window and the Alpine orogen. It is shown that diachronous exhumation of the Tauern Window was indeed related to this fragmentation.

2. Geological setting

The Tauern Window in the Eastern Alps contains an almost complete record of Alpine mountain building, from Early Mesozoic rifting and

spreading, through Tethyan subduction and Adria–Europe collision, to indentation (e.g., Trümpy, 1973; Dal Piaz, 1999; Schmid et al., 2004). The orogenic evolution of units in the Tauern Window is divided into five tectonometamorphic phases that were broadly continuous in Late Cretaceous to Miocene times (Schmid et al., 2013): (D1) southward subduction of Alpine Tethys represented by the Glockner Nappe System (green unit in Fig. 1); (D2) thrusting of the Glockner Nappe System onto the distal European margin represented by the Modereck Nappe System (blue unit in Fig. 1); (D3) isoclinal folding of this nappe stack during continued thrusting onto the European margin; (D4) formation of a duplex in the accreting European margin (Venediger Nappe System, pink units in Fig. 1) followed by Barrow-type metamorphism (Tauernkristallisation; e.g., Sander, 1911; Droop, 1985; Hoinkes et al., 1999; Dachs et al., 2005) and Periadriatic magmatism (e.g., Rosenberg, 2004); (D5) indentation of the Alpine orogenic crust by the Austroalpine units at the leading edge of the Adriatic indenter (Scharf et al., 2013a; Schneider et al., submitted for publication) represented by the Southern Alps (yellow unit in Fig. 1). Indentation involved coeval doming as well as E–W directed orogen-parallel normal faulting. Together, these structures accommodated orogen-normal shortening and lateral (eastward) escape of orogenic crust away from the front of the indenter (Scharf et al., 2013a; see evolutionary cross sections in Fig. 13 of Schmid et al., 2013).

It is important to note that by the beginning of Adria–Europe convergence in Late Cretaceous time, most of the Austroalpine units lying above and to the south of the Penninic nappe pile had already cooled to below 300 °C (e.g., Schuster et al., 2004). This rendered the units between the Tauern Window and Periadriatic Fault semi-rigid blocks which were exhumed and deformed during the advanced stages of orogenesis, as described below (Ratschbacher et al., 1991b; Stöckhert et al., 1999; Mancktelow et al., 2001; Linzer et al., 2002). Indentation of the Eastern Alps by the Southern Alps was accommodated largely by the sinistral transpressional Giudicarie Belt (GB in Fig. 1), which separates the eastern part of the Adriatic indenter from the somewhat older Oligo–Miocene western indenter and crustal wedge in the Central and Western Alps (e.g., Schmid et al., 2004; Handy et al., 2015). The western Adriatic indenter is not regarded further as it is not relevant to indentation in the Eastern Tauern Window.

The Tauern Window contains two domes: the Western Tauern Dome and the Eastern Tauern Dome (Fig. 1) that deform the D4 nappe stack and coincide with concentric isograds and maximum temperature lines (Fig. 1). The ETD is characterized by two D5 subdomes that fold the earlier D2, D3 and D4 collisional structures (Figs. 1 and 4): (1) the Hochalm Subdome, a broad box-shaped antiform that affects the D4 Göss, Hochalm and Romate nappes as well as the overlying D2 and D3 Glockner and Modereck nappe systems; and (2) a tight elongate fold with doubly plunging axes, the Sonnblick Subdome, which folds the Sonnblick Nappe as well as the Glockner and Modereck Nappe systems. The Sonnblick Lamellae (Fig. 2, Exner, 1962, 1964) is the highly sheared equivalent of the Sonnblick Subdome which runs parallel to the Mallnitz Synform (Kober, 1920), an acylindrical D5 fold, which tightens from NW to SE and separates the Hochalm and Sonnblick subdomes. The D5 Sonnblick Lamellae and Mallnitz Synform are progressively sheared to the SE, forming a mylonitic belt that bends into concordance with the SE-dipping, low-angle Katschberg Normal Fault (Fig. 2, KNF, e.g., Genser and Neubauer, 1989; Becker, 1993; Scharf et al., 2013a). The WTD and ETD were kinematically linked to large, conjugate strike-slip faults, in particular for the WTD, the sinistral Salzach–Ennstal–Mariazell–Puchberg (SEMP) Fault (e.g., Linzer et al., 2002; Rosenberg and Schneider, 2008), the dextral Periadriatic Fault (PF, Müller, 1998; Müller et al., 2001; Läufer et al., 1997) and the Mölltal Fault (MF, e.g., Kurz and Neubauer, 1996; Linzer et al., 2002) that together accommodated lateral eastward orogenic extrusion of the Alpine orogen (Ratschbacher et al., 1991b) towards the Miocene Pannonian Basin (e.g., Horvath et al., 2006). The contrast in D5 structural style within the Tauern Window, as well as the role of these conjugate strike-slip faults are discussed again below where the response of the Alpine collisional edifice to Adriatic indentation is considered in the light of new geochronological data.

3. Sample description

The samples dated in this study are listed in Table 1. They cover most of the ETD and also traverse the main D5 structures in the area where age data have been missing until now. Different lithologies were analyzed to determine the effect of the bulk rock composition on the age values.

Most samples come from the Subpenninic nappes rather than the Penninic Glockner Nappe System due to the widespread lack of biotite in the latter. The Glockner Nappe System contains ophiolitic slices and a large volume of Jurassic to Early Cretaceous calcareous metapelitic schist (so-called "Bündnerschiefer", Pestal et al., 2009) with pervasive greenschist-facies fabrics. The Glockner Nappe System is generally subdivided into two imbricates (not distinguished in Fig. 2), a tectonically lower slice with rare relics of subduction-related metamorphism (pseudomorphs after lawsonite, Pestal et al., 2009) termed the Glockner Nappe "sensu stricto" (Kolm Nappe of Exner, 1984), and a higher slice without such relics but containing metagabbroic dykes (Rauris Nappe, Exner, 1984; Pestal and Hellerschmidt-Alber, 2011; Favaro and Schuster, 2012). The three samples collected for this paper came from the Glockner Nappe sensu stricto, which however, were void of high-pressure relics.

The samples used for $^{87}Rb/^{87}Sr$ dating of muscovite and biotite were collected from basement and pre-Mesozoic cover units of the Venediger Nappe System (Fig. 2). The basement protoliths are mostly Variscan to post-Variscan (late Paleozoic) intrusives, including granitic augengneiss from the Sonnblick Nappe (Fig. 3a), syenitic gneiss from the Romate Nappe (Fig. 3b) and other orthogneisses (Fig. 3c) which intruded pre-Variscan paragneisses. These pre-Variscan host rocks are locally known as the "Altes Dach" or "Old Roof" (Kober, 1920; Staub, 1924; Exner, 1962, 1964).

Samples of the post-Variscan, pre-Mesozoic cover of all these basement rocks (Table 1) are locally very aluminous and contain abundant white mica, garnet, chloritoid and locally staurolite (Figs. 3d, 4). These silver to shiny greenish schists, part of the Woisken Schist Complex in the sense of Kober (1920), are quite striking to behold and are thought to have been deposited in Permian time because they are not intruded by Variscan dykes and are stratigraphically overlain by Mesozoic sediments (e.g., the Jurassic Hochstegen Marble and Early Cretaceous Brennkogel Schists; Pestal et al., 2009; Favaro and Schuster, 2012). Therefore, the amphibolite-facies assemblage in the Woisken Schist Complex must be Alpine and, indeed, overgrows the S4 foliation as shown in Fig. 4.

4. Analytical methods: Sample preparation for $^{87}Rb/^{87}Sr$ and $^{147}Sm/^{144}Nd$ dating

The samples were mechanically prepared for $^{87}Rb/^{87}Sr$ and $^{147}Sm/^{144}Nd$ isotope analyses at the Geological Survey of Austria in Vienna. Before separating the minerals, their weathered surfaces were removed from the sample material. Minerals were separated by the standard methods of crushing, grinding, sieving and magnetic separation. Garnet and chloritoid separates were hand-picked under the binocular microscope from sieve fractions of 0.2–0.3 mm and were cleaned in distilled water and acetone. Garnet was further leached in 6n HCl at 100 °C for several hours. Samples used for dissolution weighed about 100 mg for whole rock powder, ~200 mg for biotite and white mica and 30–45 mg for garnet and chloritoid. Chemical preparation was performed at the Geological Survey of Austria in Vienna and at the Department of Lithospheric Research at the University of Vienna. The chemical sample preparation follows the procedure described by Sölva et al. (2005). Element concentrations were determined by isotope

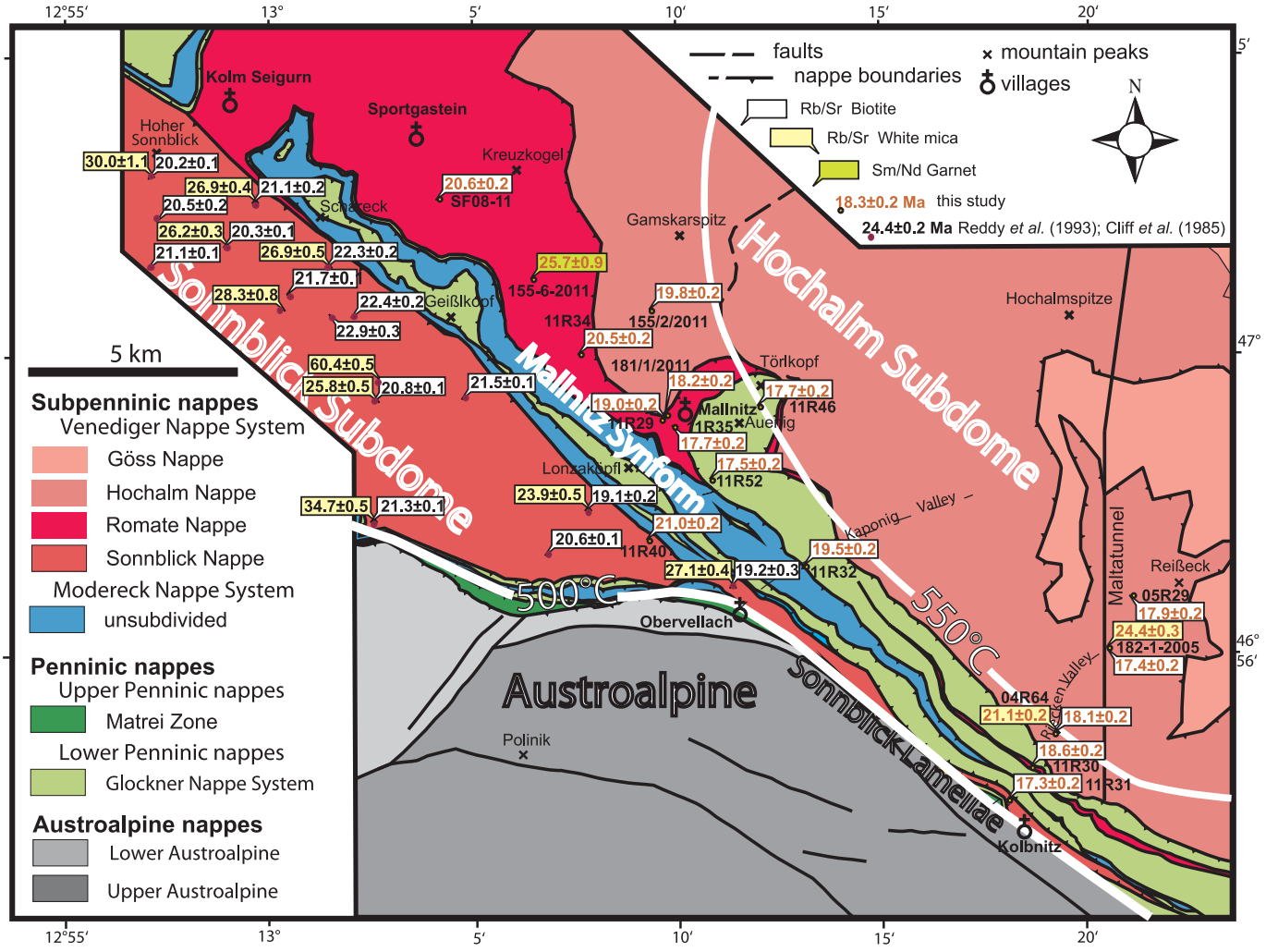

Fig. 2. Tectonic map of the study area delimited by the box in Fig. 1. The map shows sample locations and ages: Orange labels = this work, black labels indicate samples of Cliff et al. (1985) and Reddy et al. (1993). Samples of the first study were collected along the Malta Tunnel. Ages from the latter two sources were calculated with the same constants as used for own data in this paper (see text).

dilution using mixed $^{147}Sm/^{150}Nd$ and $^{84}Rb/^{87}Sr$ spikes. Total procedural blanks are ≤300 pg for Nd and Sm and ≤1 ng for Rb and Sr.

Rb ratios were measured at the Department of Geological Sciences, University of Vienna with a Finnigan® MAT 262, whereas Sr, Sm and Nd ratios were analyzed with a ThermoFinnigan® Triton TI TIMS. All elements were run from Re double filaments, except Rb which was evaporated from a Ta single filament. During measuring, the La Jolla standard yielded $^{143}Nd/^{144}Nd = 0.511841 \pm 1$ (n = 13, 2σm) on the Triton TI, whereas standard NBS987 yielded a ratio of $^{86}Sr/^{87}Sr = 0.710270 \pm 3$ (n = 12, 2σm) and 0.710274 ± 2 (n = 21, 2σm) respectively was determined. Errors of 1% were determined for the $^{87}Rb/^{86}Sr$ and $^{147}Sm/^{144}Nd$ ratios based on interactive sample analysis and spike recalibration. Ages were calculated with the software ISOPLOT/Ex (Ludwig, 2001; 2003) using the Sm- and Rb-decay constants of 6.54×10^{-12} a^{-1} and 1.42×10^{-11} a^{-1}, respectively.

5. Results

5.1. $^{147}Sm/^{144}Nd$ garnet ages

Sample 155-6-2011 (location in Table 1 and Fig. 2) is ideally suited to place an upper age limit on the Barrow-type, amphibolite-facies metamorphism (Tauernkristallisation) because it comes from post-Variscan cover and contains both garnet and chloritoid that overgrow the folded S4 foliation formed during duplex formation in the Venediger Nappe System (Fig. 4). The results of the $^{147}Sm/^{144}Nd$ measurements are given in Table 2.

Two fractions of garnet (Grt_1, Grt_2), chloritoid (Cld) and whole rock (WR) were analyzed. The whole rock is characterized by a $\varepsilon 0Nd_{(CHUR)}$ of 5.2, a $^{147}Sm/^{144}Nd$ ratio of ~0.14 and has Sm (33.5 ppm) and Nd (7.81 ppm) contents that are in the range typical for metapelites (McCullogh and Wasserburg, 1978). Both garnet fractions show low concentrations of Sm (~1 ppm) and Nd (~0.4 ppm) and remarkably high $^{147}Sm/^{144}Nd$ ratios of >1.3 and >1.8, respectively (Table 2). The calculated isochron defines an age of 25.7 ± 0.9 Ma (Fig. 4).

5.2. $^{87}Rb/^{87}Sr$ micas ages

Biotite and whole rock (WR) were analyzed in a total of fifteen samples, and two of these samples were also analyzed for white mica (Table 1). Whole rocks, as well as the corresponding biotite separates, have a broad range of Rb and Sr content and the biotites exhibit a wide range of $^{87}Rb/^{86}Sr$ ratios (50–700). The $^{87}Rb/^{87}Sr$ ages and analyses are listed in Table 3. In the following, we discuss the results with regard to the different D5 structures of the ETD.

5.2.1. Hochalm Subdome

All ten samples analyzed come from the southwestern part of the Hochalm Subdome adjacent to the Mallnitz Synform, but away from (north of) areas affected by pervasive F5 folding and S5 schistosity.

Table 1
Investigated samples and relevant information (coordinates: WGS 84).

Sample nr.	Method Tc	Lithology	Lithostratigraphy	Nappe	Peak T	Locality	N	E
Penninic nappes/Glockner Nappe System								
11R32	Rb–Sr bt 300 °C	Greenschist		Glockner Nappe sensu stricto	500–550 °C	Kaponik valley, E′ Obervellach	46° 57′ 00.6″	13° 13′ 06.5″
11R46	Rb–Sr bt 300 °C	Prasenite		Glockner Nappe sensu stricto	500–550 °C	Auenig, E′ Mallnitz	46° 59′ 32.9″	13° 11′ 58.9″
11R52	Rb–Sr bt 300 °C	Prasenite		Glockner Nappe sensu stricto	500–550 °C	Auenig, E′ Mallnitz	46° 58′ 28.2″	13° 10′ 41.4″
Subpenninic nappes/Venediger Nappe System								
11R31	Rb–Sr bt 300 °C	Augengneiss	Sonnblick augengneiss	Sonnblick Nappe	500–550 °C	E′ Kolbnitz	46° 53′ 13.7″	13° 18′ 03.8″
11R40	Rb–Sr bt 300 °C	Micaschist		Sonnblick Nappe	500–550 °C	W′ Obervellach	46° 56′ 39,0″	13° 11′ 23.3″
11R29	Rb–Sr bt 300 °C	Syenitic orthogneiss	Romate orthogneiss	Romate Nappe	500–550 °C	W′ Mallnitz	46° 59′ 22.8″	13° 09′ 56.8″
11R30	Rb–Sr bt 300 °C	Grt-mica schist		Romate Nappe	500–550 °C	Riekengraben, E′ Kolbnitz	46° 53′ 51.2″	13° 18′ 39.7″
11R34	Rb–Sr bt 300 °C	Syenitic orthogneiss	Romate orthogneiss	Romate Nappe	500–550 °C	NW′ Mallnitz	47° 00′ 09.7″	13° 07′ 48.2″
11R35	Rb–Sr bt 300 °C	Grt mica schist	Woisken Schist Complex	Romate Nappe	500–550 °C	W′ Mallnitz	46° 59′ 16.4″	13° 09′ 53.7″
SF08–11	Rb–Sr bt 300 °C	Syenitic orthogneiss	Romate orthogneiss	Romate Nappe	500–550 °C	Sportgastein	47° 02′ 23.7″	13° 04′ 10.7″
155/6/2011	Sm–Nd grt 500°	Grt-chloritoid mica schist	Woisken Schist Complex	Romate Nappe	500–550 °C	NW′ Mallnitz	47° 01′ 29.3″	13° 06′ 18.4″
181/1/2011	Rb–Sr bt 300 °C	Syenitic orthogneiss	Romate orthogneiss	Romate Nappe	500–550 °C	NW′ Mallnitz	46° 59′ 20.1″	13° 09′ 52.1″
155/2/2011	Rb–Sr bt 300 °C	Granitic orthogneiss		Hochalm Nappe	≥550°	N′ Mallnitz	47° 00′ 38.4″	13° 09′ 27.9″
05R29	Rb–Sr bt 300 °C	Grt-bearing granite		Hochalm Nappe	≥550°	Riekengraben, NE′ Kolbnitz	46° 55′ 41.7″	13° 20′ 01.4″
04R64	Rb–Sr bt/wm 300, 500 °C	Granitic orthogneiss		Hochalm Nappe	≥550°	NE′ Kolbnitz	46° 54′ 12.1″	13° 19′ 13.9″
182/1/2005	Rb–Sr bt/wm 300, 500 °C	Two-mica granitic gneiss	Schönanger orthogneiss	Hochalm Nappe	≥550°	Riekengraben, E′ Kolbnitz	46° 56′ 42.7″	13° 20′ 19.9″

The micas in these samples thus define older foliations, usually S4 which was related to nappe stacking and the formation of the Venediger Duplex. Two of these samples experienced more than 550 °C (Fig. 2) defined by peak-temperature assemblages of the Tauernkristallisation (Hoinkes et al., 1999) and by Raman microspectroscopy on carbonaceous material (Scharf et al., 2013b). The highest temperature in the area, 610 °C, is measured in the core of the ETD just east of the area shown in Fig. 2 (Scharf et al., 2013b).

These two samples yield biotite ages in the narrow range of 17.9 to 17.4 ± 0.2 Ma and are the youngest biotite ages from the Hochalm Subdome. White mica from the white mica-biotite granitic gneiss (182-1-2005; Schönangergneiss, central part of the Hochalm Subdome) yields 24.4 ± 0.3 Ma, whereas another muscovite from an orthogneiss from the southwestern margin of the Hochalm Subdome near Kolbnitz (04R64) yields 21.1 ± 0.2 Ma. Both white mica ages are older than the biotite ages from the same sample.

The remaining eight samples come from areas between the 500° and 550 °C isotherms and yield biotite ages between 17.7 ± 0.2 Ma and 20.6 ± 0.2 Ma. The scatter in ages is remarkably small given the different protoliths, foliations and $^{87}Rb/^{86}Sr$ systematics of these samples (Table 3). Two of these samples come from the rim of the Hochalm Nappe, one in the proximity of Kolbnitz (04R64) and one north of Mallnitz (155-2-2011, Gamskarspitz). Four samples are of relatively undeformed, biotite-rich Romate syenitic gneiss, whereas two come from the post-Variscan cover of the Romate Nappe (Permian Woisken Schist Complex). Only sample 04R64 has a composite S4–S5 foliation due to its proximity to the KNF (Scharf et al., 2013a), whereas sample 155-2-2011 is located just below the contact with the Romate gneiss and preserves a strong D4 foliation. The micas in the syenitic gneiss define older, pre-D4 foliations, whereas the garnet-bearing muscovite schist (11R35, Fig. 3d) collected near the Venediger Duplex roof thrust has a strong S4 foliation comprising white mica, biotite and retrograde chlorite. The biotite concentrate from this schist has a high Sr content (17 ppm) resulting in a low $^{87}Rb/^{86}Sr$ ratio of ~100. This high Sr content reflects the presence of tiny Sr-rich inclusions, most probably of apatite.

Sample (11R30) from the Kolbnitz area (Fig. 2) contains biotite in a quartz vein. These extensional veins trend northeast–southwest and have been well studied because of their gold content ("Tauerngold"; Feitzinger and Paar, 1991). The biotite is highly radiogenic ($^{87}Rb/^{86}Sr$ ~700) and its orientation parallel to the KNF suggests that it formed during D5 orogen-parallel extension.

5.2.2. Sonnblick Subdome

A paragneiss (sample 11R40) from the Sonnblick Nappe (location north of Obervellach, Fig. 2) and an augengneiss from the "Sonnblick Lamellae" close to Kolbnitz (sample 11R31, Figs. 2, 3a) contain biotite that defines the S5 foliation in the Katschberg Shear Zone System. The biotites from both samples have high Sr contents (17 and 34 ppm) and correspondingly low $^{87}Rb/^{86}Sr$ ratios (56 and 74 ppm), pointing to the presence of Sr-rich inclusions within the biotites. The calculated ages are 21.0 ± 0.2 Ma for the paragneiss near Obervellach, and 17.3 ± 0.2 Ma for the augengneiss of the Sonnblick Lamellae.

5.2.3. Mallnitz Synform

Sample 11R32 from the Kaponig Valley (Fig. 2) is a chlorite-schist with aggregates of biotite up to several millimeters long that are oriented subparallel to axial planes of F5 folds near the mylonitic belt that connects along strike to the SE with the KNF. Samples 11R46 and 11R52 from Auernig (Fig. 2) are prasinites (epidote, plagioclase, greenish-brown biotite, chlorite and minor quartz, tourmaline and apatite). The biotites in these samples are probably pre-D4 because they originate in the isoclinally folded (D3) Glockner Nappe System that overlies the D4 roof thrust of the Venediger Duplex. All three samples have biotites characterized by low Sr content (~4 ppm), relatively low Rb content (200–380 ppm) and by $^{87}Rb/^{86}Sr$ ratios of 150–260. The biotite age values are in the range of 17.5–19.5 ± 0.2 Ma.

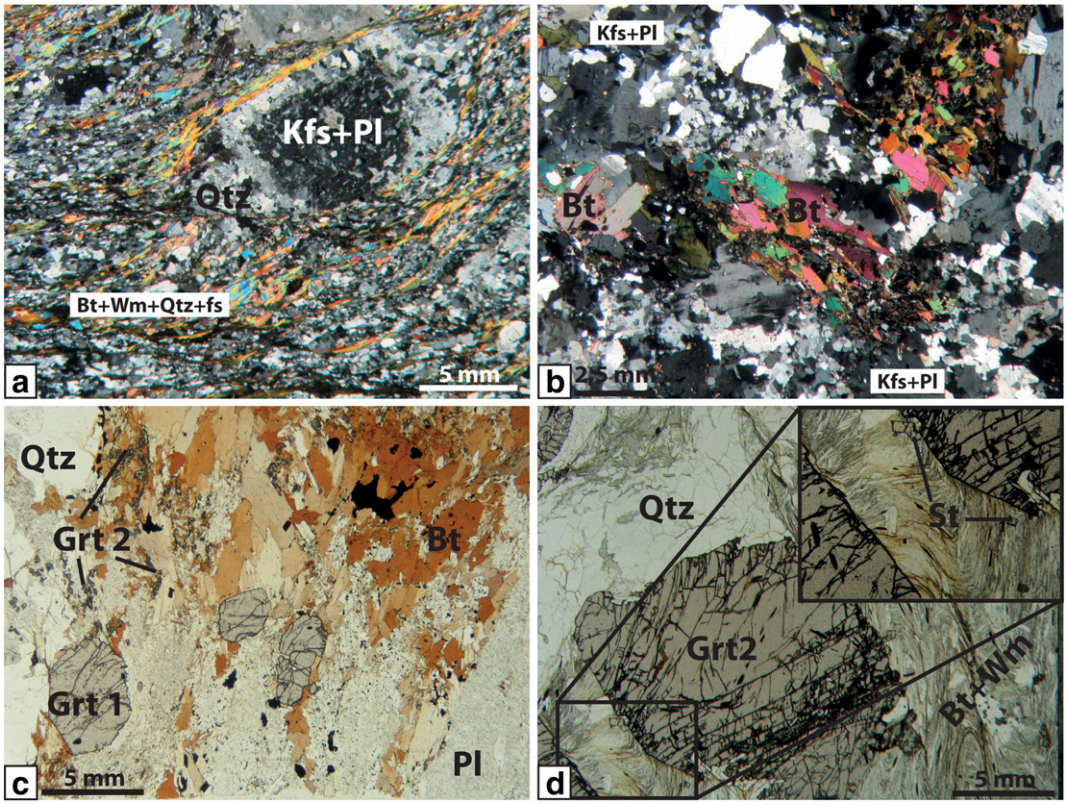

Fig. 3. Microstructures indicative of deformation at peak-temperature conditions in the ETD: (a) Sonnblick augengneiss (sample 11R31) with S5 is defined by biotite and white mica, interpreted to have equilibrated at or below ~500 °C (see text). Cores of K-feldspar augen have perthitic exolutions and inclusions of euhedral plagioclase crystals, whereas rims exhibit dynamic recrystallization of feldspar intergrown with quartz in the pressure shadows; (b) Romate syenitic orthogneiss (sample SF08–11) in the northwestern part of the Hochalm Subdome shows dynamic recrystallization of feldspar and of minor amounts of quartz; dynamic recrystallization interpreted to be related to D4; (c) granite from the Hochalm Subdome (sample 05R29) containing inclusion-free magmatic garnet (Grt1) overgrown by fine grains of metamorphic garnet (Grt2) in contact with biotite; Grt2 is interpreted to have grown at peak temperatures of ≥500 °C; (d) Grt2 from post-Variscan cover (Woisken Schist Complex, sample 11R35) of the Romate Gneiss with F4-folded matrix comprising peak-temperature assemblage of white mica, biotite and staurolite (see inset). This assemblage is interpreted to have grown during the Tauernkristallisation.

6. Discussion

6.1. Age of Alpine peak-temperature conditions

The age of the Barrow-type thermal event (Tauernkristallisation) in the Tauern Window is broadly constrained by cross-cutting relationships: Peak-temperature (peak-T) lines form a lopsided concentric pattern in the ETD that cuts and therefore post-dates D4 nappe contacts (Fig. 1, Droop, 2013; Scharf et al., 2013b). Maximum temperatures range from ~612 °C in the core of the EDT to only ~450 °C along the KNF (Scharf et al., 2013b). The concentric pattern itself reflects D5 doming in the Hochalm Subdome, while the parallelism of peak-T lines to the KNF (Fig. 1) is attributed to shearing of isotherms into concordance with the footwall of the KNF (Scharf et al., 2013b). These overprinting relations indicate that the Tauernkristallisation occurred prior to the activity of the KNF in early Miocene time (Scharf et al., 2013a). The

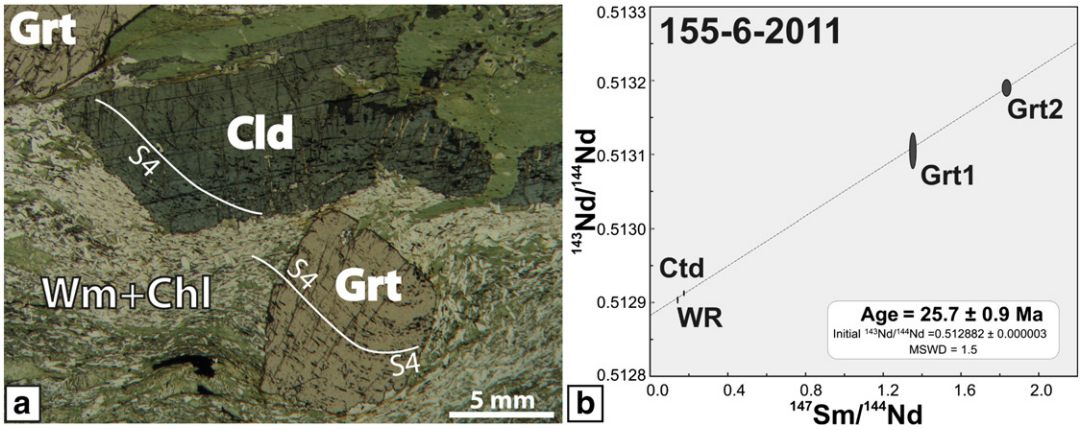

Fig. 4. (a) Garnet-chloritoid mica schist from the post-Variscan cover in the western part of the Hochalm Subdome (Woisken Schist Complex, sample 155-6-2011). Sample contains quartz, muscovite, biotite, garnet and minor chlorite, staurolite, chloritoid and epidote. Garnet (Grt) and chloritoid (Cld) are interpreted to overgrow the folded S4 foliation defined mainly by white mica; (b) $^{143}Nd/^{144}Nd$ vs $^{147}Sm/^{144}Nd$ plot for two garnet fractions (Grt1, Grt2), chloritoid (Ctd) and whole rock (WR).

Table 2
$^{147}Sm/^{144}Nd$ isotopic data for a garnet-chloritoid mica schist from the post-Variscan cover in the western part of the Hochalm Subdome (Woisken Schist Complex, sample 155-6-2011).

Sample/material		$^{143}Nd/^{144}Nd$	$\pm 2\sigma_m$	Nd [ppm]	Sm [ppm]	$^{147}Sm/^{144}Nd$	$\varepsilon 0Nd_{(Chur)}$
Subpenninic nappes/Venediger Nappe System							
155/6/2011	WR	0,512904	±0.000003	33,52	7,806	0,1408	5,2
155/6/2011	Ctd	0,512913	±0.000003	4,005	1,149	0,1734	5,4
155/6/2011	Grt1	0,513105	±0.000020	0,439	0,982	1,3518	9,1
155/6/2011	Grt2	0,513190	±0.000009	0,401	1,216	1,8340	10,8

Tauernkristallisation is therefore interpreted as the thermal response to crustal thickening by D4 nappe stacking and duplex formation during Adria–Europe collision (Kurz et al., 2008; Schmid et al., 2013).

Duplex formation must post-date subduction of the European plate and pre-date early exhumation of high-pressure metamorphic units in the Tauern Window, including the Glockner Nappe sensu stricto, the Eclogite Zone and part of the Modereck Nappe System (Fig. 1). However, the age of the high-pressure metamorphism in these units is controversial, with estimates ranging from 42–38 Ma ($^{40}Ar/^{39}Ar$ phengite, Ratschbacher et al., 2004; Kurz et al., 2008) to 36–32 Ma ($^{87}Rb/^{87}Sr$ white mica, Glodny et al., 2005; Lu/Hf in garnet-bearing assemblage, Nagel et al., 2013).

In view of this uncertainty, the best approach to dating the Tauernkristallisation employs isotopic systems with closure temperatures (T_c) higher than or near the peak temperatures recorded in the Tauern Window. Where the peak-T exceeded 500–550 °C in the WTD, white micas yield 29 ± 2 Ma, 31 ± 5 Ma, ($^{87}Rb/^{87}Sr$ white mica, T_c ~550 °C, Satir, 1975) and 32 ± 2 Ma (K/Ar white mica, T_c ~420 °C, Satir, 1975; Thöni, 1980). These ages are in good agreement with new U/Pb apatite ages mostly between 31 and 29 Ma in the core of the WTD (T_c ~450 °C, Schneider et al., 2015). All of these ages can be interpreted as cooling ages that somewhat post-date the thermal peak of Tauernkristallisation because the closure temperature of the systems used was slightly less than the maximum temperature recorded in the rocks. Other studies on samples closer to the Brenner Normal Fault yield slightly younger white mica ages in the range of 30–28 Ma which are interpreted as cooling ages following the Tauernkristallisation event (e.g., Lambert, 1970; Selverstone, 1985; Raith et al., 1978; Ratschbacher et al., 2004).

A detailed study of a single, 6-cm diameter synkinematic garnet (Pollington and Baxter, 2010) from a shear zone in the WTD indicates garnet growth at temperatures of at least 500 °C from 28 to 20 Ma, with an increased growth rate at about 25 Ma. According to Selverstone et al. (1991) this shear zone experienced significant mass- (<50%) and volume- (<60%) loss related to fluid flow between 20 and 30 Ma (Barnes et al., 2004). These observations are in agreement with studies on steeply dipping shear zones in the WTD by Schneider et al. (2013).

In the southwestern part of the ETD (Sonnblick Subdome), where the peak-T of 510 °C (Droop, 2013) is about the same as the T_c of the $^{87}Rb/^{87}Sr$ white mica system, Reddy et al. (1993) interpreted their

Table 3
$^{87}Rb/^{87}Sr$ isotopic data and ages.

Sample	Material	$^{87}Sr/^{86}Sr \pm 2\sigma_m$	Rb [ppm]	Sr [ppm]	$^{87}Rb/^{86}Sr$	Age $\pm 2\sigma_m$ [Ma]
Penninic nappes/Glockner Nappe System						
11R32	WR	0.707927 ± 0.000003	322.9	379.2	2.4637	
11R32	Bt	0.778776 ± 0.000004	380.3	4.286	258.52	19.5 ± 0.2
11R46	WR	0.706317 ± 0.000003	25.3	359.5	0.2034	
11R46	Bt	0.743767 ± 0.000004	204.6	3.977	149.36	17.7 ± 0.2
11R52	WR	0.705304 ± 0.000003	47.7	138.4	0.9968	
11R52	Bt	0.749119 ± 0.000003	234.7	3.855	176.92	17.5 ± 0.2
Subpenninic nappes/Venediger Nappe System						
11R31	WR	0.707636 ± 0.000004	201.4	874.7	0.6665	
11R31	Bt	0.721275 ± 0.000004	681.1	35.12	56.198	17.3 ± 0.2
11R40	WR	0.707160 ± 0.000004	121.5	519.0	0.6774	
11R40	Bt	0.729269 ± 0.000004	444.9	17.24	74.834	21.0 ± 0.2
11R29	WR	0.712428 ± 0.000004	250.3	580.0	1.2494	
11R29	Bt	0.879310 ± 0.000005	538.9	5.260	301.45	19.0 ± 0.2
11R30	WR	0.722992 ± 0.000004	331.3	110.2	8.7166	
11R30	Bt	0.903758 ± 0.000004	907.3	3.866	692.25	18.6 ± 0.2
11R34	WR	0.713052 ± 0.000004	269.1	677.2	1.1506	
11R34	Bt	0.826504 ± 0.000004	1356	10.14	391.65	20.5 ± 0.2
11R35	WR	0.714292 ± 0.000004	204.0	157.4	3.7542	
11R35	Bt	0.738105 ± 0.000004	605.7	17.84	98.544	17.7 ± 0.2
SF08–11	WR	0.712322 ± 0.000004	396.3	614.9	1.8657	
SF08–11	Bt	0.818404 ± 0.000004	1560	12.54	363.78	20.6 ± 0.2
181/1/2011	WR	0.712058 ± 0.000004	374.0	978.1	1.1070	
181/1/2011	Bt	0.812299 ± 0.000004	1483	11.15	389.03	18.2 ± 0.2
155/2/2011	WR	0.709734 ± 0.000003	145.8	561.6	0.7516	
155/2/2011	Bt	0.770631 ± 0.000004	829.8	11.14	216.98	19.8 ± 0.2
05R29	WR	0.716372 ± 0.000004	141.1	272.2	1.5015	
05R29	Bt	0.855328 ± 0.000005	868.4	4.651	548.17	17.9 ± 0.2
04R64	WR	0.711393 ± 0.000004	165.0	284.8	1.6775	
04R64	Bt	0.735008 ± 0.000018	981.4	30.42	93.613	18.1 ± 0.2
04R64[a]	Ms	0.730748 ± 0.000015	561.8	24.61	66.227	21.1 ± 0.2
182/1/2005	WR	0.737378 ± 0.000004	238.9	83.46	8.3098	
182/1/2005	Bt	1.547216 ± 0.000702	1335	1.273	3283.2	17.4 ± 0.2
182/1/2005[a]	Ms	0.850518 ± 0.000009	825.3	7.225	335.21	24.4 ± 0.3

[a] Data included also in Scharf et al. (submitted for publication Tectonophysics).

ages between 30 and 24 Ma either as formation ages during the Tauernkristallisation or as cooling ages shortly thereafter. In the larger Hochalm Subdome where peak-T exceeded 550 °C, the two new $^{87}Rb/^{87}Sr$ white mica ages in this study (Table 1, Fig. 2) as well as the previously published ages of Cliff et al. (1985; Fig. 2) are consistently younger (24–21 Ma). These are therefore interpreted as cooling ages after the peak of Tauernkristallisation. Note that the $^{87}Rb/^{87}Sr$ white mica ages in this study are more variable than the biotite ages from the same samples (04R64, 182-1-2005), a phenomenon also observed in the white mica ages of Cliff et al. (1985). This variability most probably reflects minor and variable amounts of Sr loss during post-peak metamorphic deformation and recrystallisation of the micas.

Other systems applied to minerals of the peak-temperature assemblage in the ETD yield ages in the narrow range of 29–27 Ma (metamorphic crystallization, Th/Pb and U/Pb allanite, Cliff et al., 1998; formation ages, $^{87}Rb/^{87}Sr$ white mica, U/Pb allanite and titanite, Inger and Cliff, 1994). These ages lie within the broad range of the white mica ages cited above.

The $^{147}Sm/^{144}Nd$ isochron age (25.7 ± 0.9 Ma) on garnet–chloritoid–whole rock in this study (Table 2) is interpreted to date the growth of the peak-temperature assemblage after the formation of S4 related to shearing during duplex formation in the Venediger Nappe System. This is seen in Fig. 4, where garnet and chloritoid overgrow a folded S4 foliation defined by fine trails of white mica. The 25.7 Ma age supports the ages of the other high-temperature systems and predates the cooling ages in the ETD.

To summarize this section, the available isotopic ages indicate that the Barrow-type thermal event in the Tauern Window lasted for about 7 Ma, beginning no later than 32 Ma (oldest $^{87}Rb/^{87}Sr$ white micas) and lasting until about 25 Ma as indicated by the $^{147}Sm/^{144}Nd$ garnet formation ages from the WTD and ETD and the youngest $^{87}Rb/^{87}Sr$ ages on white micas. This suggests that crustal thickening during Adria–Europe collision started before 32 Ma. This fits well with geological evidence for thickening of continental crust as manifested by the transition from an underfilled trench with predominantly flysch in Eocene time, to Molasse-type sedimentation in the Alpine continental foredeep beginning in latest Eocene to early Oligocene time (see Kurz et al., 2008; Handy et al., 2010, 2015; Schmid et al., 2013).

6.2. Cooling of the Eastern Tauern Dome

All new $^{87}Rb/^{87}Sr$ biotite ages are from samples that experienced peak metamorphic temperatures of 500 °C or more, well above the T_c of the $^{87}Rb/^{87}Sr$ system in biotite (300 °C, Jäger et al., 1967; Del Moro et al., 1982), so these ages are clearly interpretable as cooling ages. Regarded together with existing isotopic ages in the literature, these ages define three distinct cooling domains in the study area, each with its own T–t cooling curve (color coded in Fig. 5a, b). It is noticeable that boundaries between these cooling domains generally trend northeast–southwest, obliquely to the major D4 nappe contacts and D5 domes, as well as to the 500 and 550 °C peak-T contours that outline the core of the ETD. In particular, the boundary between cooling domains 1 and 2 cuts across the Mallnitz Synform, while that between domains 2 and 3 overprints the D5 sheared contact between the Hochalm Subdome and Sonnblick Lamellae (Fig. 5a). The curves themselves record cooling from 500° to about 240 °C and the age of this cooling is seen to become progressively younger going from the northwest (domain 1) to the southeast (domain 3) towards the footwall of the Katschberg Normal Fault (Fig. 5b). Judging from the average slopes of the T–t curves in Fig. 5b, the average cooling rate was about 33 °C Ma^{-1} in all domains. Constraints from lower temperature systems are sparse: zircon fission track ages show cooling of the ETD to below 240 °C between 19 and 11 Ma (Yamada et al., 1995; Dunkl et al., 2003; Wölfler et al., 2008, 2012; Bertrand, 2013), and apatite fission track ages to below ~125 °C between 27 and 3 Ma (Staufenberg, 1987; Foeken et al., 2007; Wölfler et al., 2008, 2012; Bertrand, 2013). Cooling in this low-temperature domain to below the viscous-frictional transition in quartz-bearing rocks (~300 °C, Stipp et al., 2002) is very poorly constrained (Scharf et al., 2013a) and sample locations are too widely spaced to resolve significant late differential cooling under subgreenschist-facies conditions within the ETD.

Deriving exhumation and exhumation rates from cooling ages is difficult in the absence of thermal modeling, which only exists for the western part of the Tauern Window (Fügenschuh et al., 1997). Without such models, a number of simplifying assumptions must be made, for example, that the average heat flow and geothermal gradient did not change significantly with time and that both heat production and heat capacity of the rocks were uniform in the exhuming nappe pile. Although none of these assumptions are well constrained, they are probably realistic in light of the fact that most samples are metagranitoids with similar rock-physical properties, including heat capacity and heat production by decay of radiogenic K, Th and U. In addition, thermal modeling of exhuming basement rocks in the WTD has shown that exhumation preceded the onset of rapid cooling by only about 2 Ma (Fügenschuh et al., 1997). The time lag between the onset of rapid exhumation and rapid cooling was probably even less in the ETD, where cooling rates (33 °C Ma^{-1}) were somewhat lower than in the WTD (45 °C Ma^{-1}), giving the exhuming rocks more time to equilibrate with the ambient thermal state of the crust.

The trend of progressively younger cooling from NW to SE in the ETD is therefore interpreted to reflect the migration of D5 exhumation during broadly coeval post-nappe doming and top-SE orogen-parallel shearing along the southeastwardly propagating KNF (Scharf et al., 2013a). The peak pressure experienced by these units during the Tauernkristallisation was 800–1000 MPa (Droop, 1985; Gipper, 2012; Hawemann, 2013), consistent with 25–30 km of exhumation for an average crustal density of 2.8 g/cm^3. Doming probably started between 30 and 25 Ma in both the Sonnblick Subdome and NW part of the Hochalm Subdome (domain 1), then began to affect the rest of the Hochalm Subdome and the Sonnblick Lamellae in the SE at 25–23 Ma (domain 2) before reaching the present-day core of the Hochalm Subdome and footwall of the KNF from 23 to 17 Ma (domain 3, Fig. 6). The 23 Ma age for the onset of this doming in domain 3 coincides exactly with the estimated age for the beginning of top-SE mylonitic shearing in the footwall of the KNF (Scharf et al., 2013a).

The obliquity of the cooling domain boundaries and the concentric peak-temperature contours in the ETD (inset to Fig. 5, see Scharf et al., 2013b; Cliff et al., 1985) indicates that these contours are not isochrons but are about 4–5 Ma older in the northwestern than in the southeastern part of the ETD. The diachronous nature of the peak-temperature contours can also be inferred on an even larger scale from cross-cutting relationships of peak-temperature contours and major D4 and D5 structures in the Tauern Window as a whole (Fig. 1): In the central part of the Window where somewhat lower peak temperatures (500–550 °C) and oldest mica cooling ages are recorded (Luth and Willingshofer, 2008), the contours follow the broadly arcuate shape of the D5 fold axes around the Tauern Window (Figs. 1, 4 of Schmid et al., 2013) and clearly cut all D4 nappe contacts. There, the peak temperatures appear to have been attained during D5. In the cores of the ETD and WTD, the concentric shape of the peak-temperature contours clearly reflects later D5 doming. At both ends of the Tauern Window these contours are modified by the Brenner and Katschberg Normal Faults, as already noted by several authors (Fügenschuh et al., 1997; Frisch et al., 2000; Luth and Willingshofer, 2008; Scharf et al., 2013b).

Taken together, these patterns suggest that doming in the central part of the Tauern Window occurred during the attainment of peak temperatures during the Tauernkristallisation whereas at the ends of the Tauern Window, doming and orogen-parallel shearing clearly occurred after this thermal peak event. This map-scale pattern of orogen-parallel migration of doming and exhumation is revisited in the next section, where the exhumation pattern implied by this migration is considered

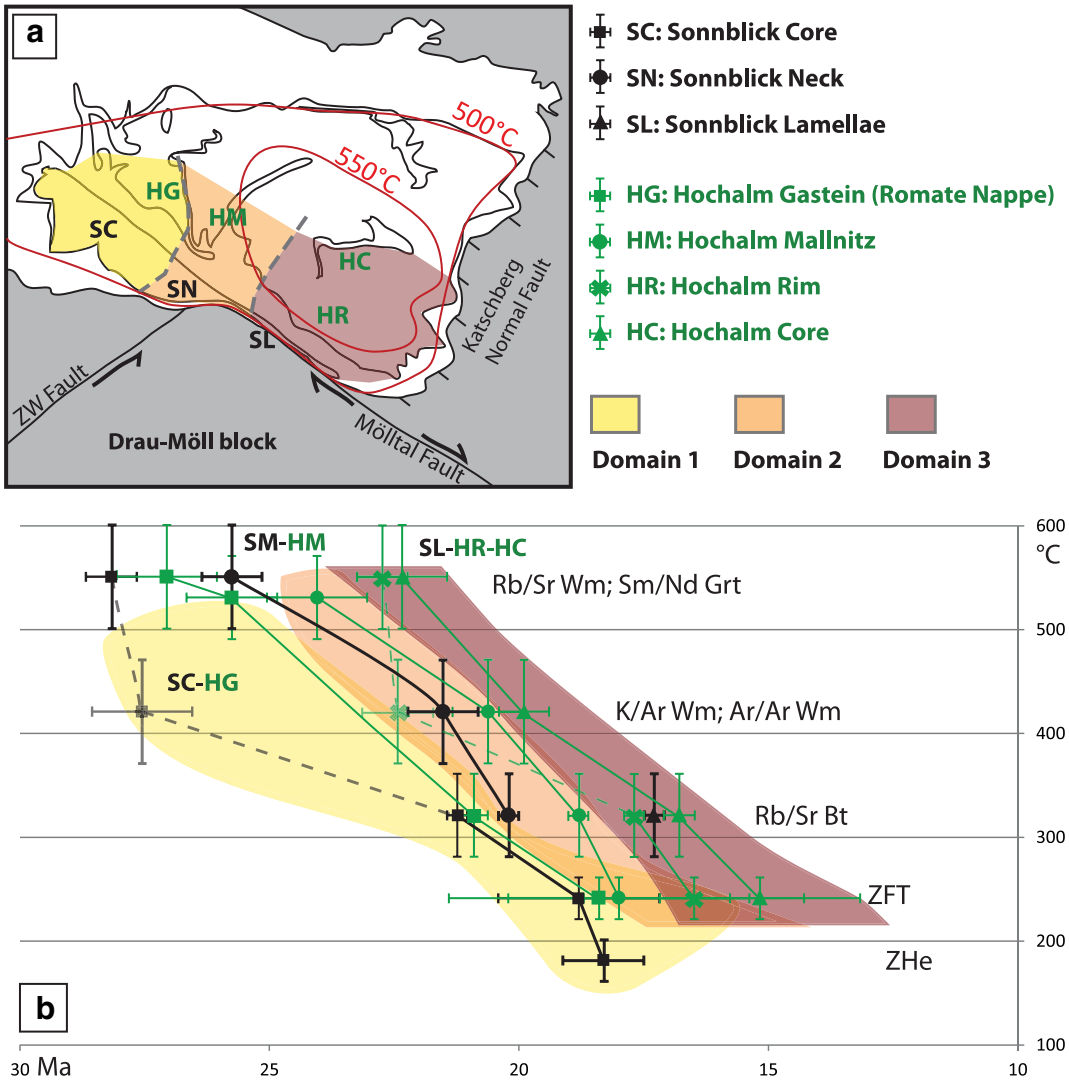

Fig. 5. Cooling patterns in the ETD, southeastern Tauern Window: (a) Map of the ETD showing three cooling domains (colored) that cut across D4 nappe contacts (thin black lines) and major D5 folds (Hochalm and Sonnblick Subdomes, Mallnitz Synform) and the peak-temperature lines related to the Tauernkristallisation. The cooling histories of these domains are defined by the T–t curves in (b); (b) temperature–time (T–t) curves for the three cooling domains in (a) with crosses indicating the errors in closure temperatures (T_c) and ages for the thermochronological systems used. Dashed parts of cooling curves connecting the ages are less well constrained (few available cooling ages) than the solid parts and probably reflect an excess argon effect. Peak-temperature contours in (a) are taken from Scharf et al. (2013b) and sources therein. Sample locations, ages and T_c values used for this figure are listed in the table and map in the Appendix A.

as a response to changing geometric boundary conditions during indentation and fragmentation of the Adriatic indenter.

We conclude this section by noting that the cooling pattern in Fig. 5 precludes earlier hypotheses reviewed in the Introduction in which the Sonnblick Subdome cooled from 500° to 300 °C before the Hochalm Subdome (Reddy et al., 1993; Cliff et al., 1985). This would imply significant vertical displacements along the intervening Mallnitz Synform, which is inconsistent with the observed subhorizontal stretching lineations and sinistral shear sense in D5 mylonites striking parallel to this synform (Scharf et al., 2013a).

6.3. The relationship of exhumation and cooling to the structural evolution of the Adriatic indenter — A model

Any model of exhumation must account for the 2–3 Ma difference in the onset of rapid cooling in the ETD and WTD, as well as along-strike migration in the age of D5 doming in the ETD. The schematic map in Fig. 6 shows how the evolving pattern of cooling of orogenic crust in the Tauern Window can be related to progressive indentation and fragmentation of the Austroalpine units along the front of the Adriatic indenter. Specifically, we propose that the migration of rapid cooling of the ETD from 500 to 300 °C reflects the migration of doming and extensional exhumation in response to exhumation and fragmentation of the Austroalpine units into the two triangular blocks, the Rieserferner and Drau–Möll blocks (Fig. 1) along the front of the Adriatic indenter (e.g., Cliff et al., 1985; Hoke, 1990; Reddy et al., 1993; Inger and Cliff, 1994; Scharf et al., 2013a). This evolution is traced schematically in Fig. 6.

The initial configuration of the Austroalpine units proposed in Fig. 6a was obtained by retrodeforming the Rieserferner and Drau–Möll blocks along the sinistral Zwischenbergen–Wöllatratten (ZWT) Fault, bringing them into their positions prior to the main stage of indentation. The ZWF accommodated about 20 km of sinistral displacement in map view according to offset of the late

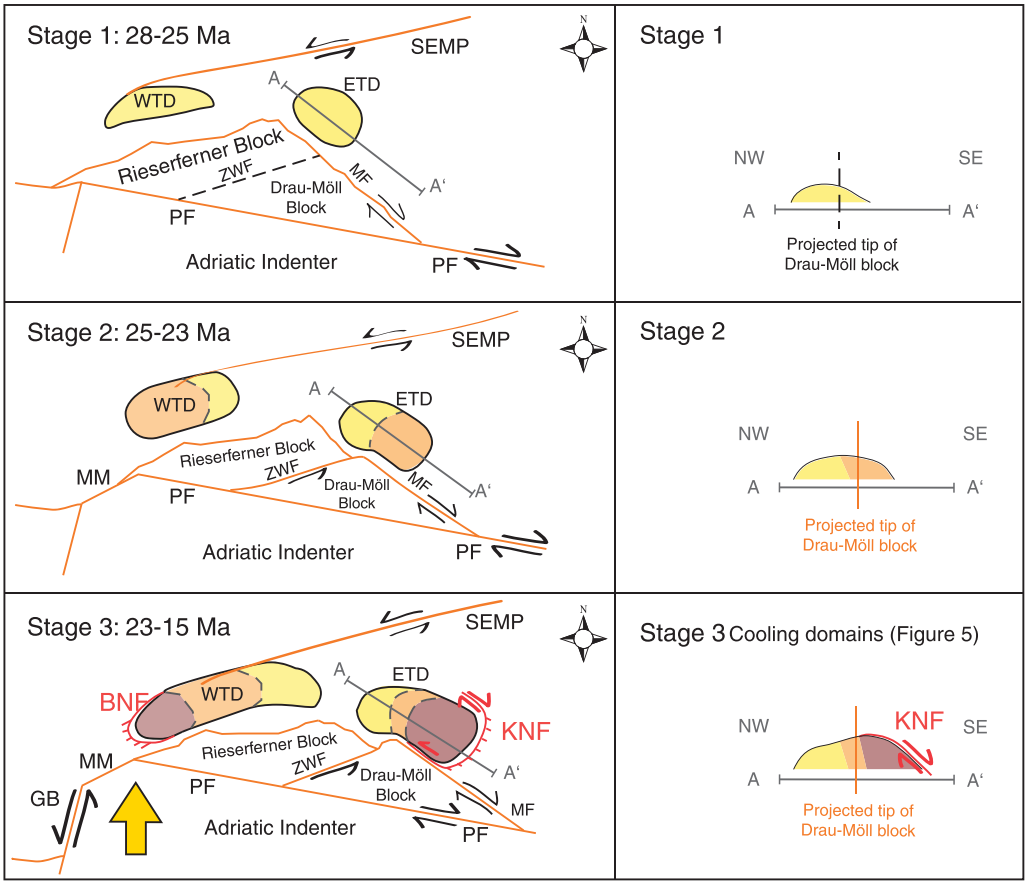

Fig. 6. Schematic maps (left column) and cross sections (right column) showing progressive fragmentation of indenting Austroalpine blocks and related migration of doming during exhumation of the ETD (see text for explanation). Colors marking the cooling domains previously shown in Fig. 5. Age intervals above the cross section for stage 3 indicate NW to SE passage of the 300 °C isotherm through the ETD according to $^{87}Rb/^{87}Sr$ biotite ages in the literature (see references in Appendix A). Abbreviations: BNF — Brenner Normal Fault, ETD — Eastern Tauern Dome, GB — Giudicarie Belt, Hochalm Subdome, KNF — Katschberg Normal Fault, MF — Mölltal Fault, MM — Meran–Mauls Fault, PF — Periadriatic Fault, Sonnblick Subdome, SEMP — Salzach–Ennstal–Mariazell–Puchberg Fault, WTD — Western Tauern Dome, ZWF — Zwischenbergen–Wöllatratten Fault. Big yellow arrows indicate motion of the Adriatic indenter with respect to stable Europe. Active faults in orange (strike-slip with arrows and normal faults in red with ticks), inactive faults in black.

Oligocene Defereggen–Antholz–Vals and Ragga–Teuchl Faults (DAV and RT in Fig. 1). These are interpreted to have originally been one through-going sinistral fault that was active during intrusion of the late Oligocene Periadriatic intrusives (age criteria in Müller et al., 2000; Mancktelow et al., 2001; Romer and Siegesmung, 2003; Wagner et al., 2006), prior to Miocene indentation (Scharf et al., 2013a and references therein). Other lithological markers are similarly offset along the ZWF (Linner et al., 2013). We note that both the Rieserferner and Drau–Möll blocks contain a number of shorter faults with smaller displacements (≤ a few km, Schuster et al., 2015), some of which offset (e.g., Iseltal Fault; Fig. 1) and even reactivate (RT, e.g. Wölfler et al., 2015) the larger, aforementioned faults. These smaller faults are interpreted to have allowed the Austroalpine blocks to deform compatibly during indentation, as discussed below.

The occurrence of deeper Periadriatic intrusives and younger Rb–Sr mica cooling ages in the Rieserferner Block (intrusive depths of 10 km, Rensen and Rieserferner plutons, Stöckhert et al., 1999; Borsi et al., 1973, 1978) than in the Drau–Möll Block (e.g., Rosenberg, 2004 and references therein) suggests that the former block was exhumed from greater depths than the latter. In addition, zircon fission track ages of 30–40 Ma (Wölfler et al., 2008, 2015) in the northern parts of the Rieserfernen and Drau–Möll blocks indicate that temperatures close to 240 °C prevailed during the Oligocene, whereas Mesozoic sediments in the southern parts of the block near the Periadriatic Fault reached only anchizonal to diagentic conditions (Rantitsch, 2001; Schuster et al., 2004). The Austroalpine blocks at the time of indentation were therefore cooler and stronger than the hot and weak Paleogene nappe stack in the Tauern Window (Genser et al., 1996; Linzer et al., 2002; Scharf et al., 2013a). Together, the restored Rieserferner and Drau–Möll blocks formed a large triangular zone along the leading edge of the Southern Alpine crust, as depicted in Fig. 6a. In addition, the entire Eastern Alpine orogenic edifice was restored about 50 km to the east, equivalent to the dextral displacement at that location due to eastward lateral escape accommodated by the Periadriatic Fault since late Oligocene time (30 Ma; Pomella et al., 2011, 2012). It is noted that this estimate is consistent with the overall trend of eastwardly increasing, post-20 Ma dextral displacement along the Periadriatic Fault; the displacement ranges from 0 km at its junction with the Meran–Mauls and Giudicarie Belt at the apex of the Southern Alpine indenter, to a maximum of about 260 km along the Mid-Hungarian Fault Zone (Fig. 1a; Handy et al., 2015). This along-strike displacement gradient is consistent with the idea that the Neogene Periadriatic Fault east of the Giudicarie Belt was a crustal stretching fault (Means, 1989) that accommodated lateral eastward escape of the far-traveled Austroalpine nappes (dark gray units in Fig. 1a, Fodor et al., 1998; Horvath et al., 2006).

Analogue modeling of indentation has shown that triangular zones of little or no deformation ("dead zones") form in front of rigid indenters between kinematic singularities at the corner or corners of the indenters (e.g., Tapponnier et al., 1986; Ratschbacher et al., 1991a; Rosenberg et al., 2007). At low strains, such dead zones are thus protected from the high differential stresses that would favor failure. However, with progressive indentation, these zones are eventually dissected by strike-slip faults and the zones fragment into smaller blocks.

In the case of the Eastern Alps, we propose that the Austroalpine crust immediately south of the Tauern Window formed such a dead zone in front of the Adriatic indenter, which is represented by the Southern Alps east of the Giudicarie Belt (Fig. 1). The southeastern corner of this indenter, at the junction of the sinistral Giudicarie Belt and the dextral Periadriatic Fault (Figs. 1, 6a), was the site of a kinematic singularity. Both of these faults were active throughout late Oligocene/Miocene time and delimited the indenter from the orogenic crust to the north (e.g., Müller, 1998; Müller et al., 2001; Läufer et al., 1997; Pomella et al., 2011, 2012; Handy et al., 2005). The Periadriatic Fault decoupled the triangular dead zone of Austroalpine crust from this indenter and facilitated eastward lateral escape of Eastern Alps, including the exhuming Cenozoic orogenic crust in the Tauern Window (Frisch et al., 1998; Linzer et al., 2002). It is important to note that this dead zone was not entirely immune to Alpine deformation and heating, as its leading edge experienced penetrative Paleogene Alpine deformation and temperature of ≥300 °C (age maps of Schuster et al., 2004; fabric map of Scharf et al., 2013a, their Fig. 8). Furthermore, as northward Adriatic indentation progressed, this zone was dissected by conjugate strike-slip faults that lead to the individuation of the semi-rigid Rieserferner and Drau–Möll blocks (Fig. 6b; Scharf et al., 2013a, their Fig. 8). The strike-slip faults bounding these blocks allowed the blocks to extend subparallel to the orogen, thus accommodating some of the northward Adriatic indentation (Frisch et al., 1998; Linzer et al., 2002).

It is proposed that the northward motion and eastward displacement of the Rieserferner and Drau–Möll blocks induced the migration of doming and KNF-related extensional exhumation in the Tauern Window away from, and to the east of, the indenter front as recorded by the cooling age pattern in this study. A key to understanding this scenario is that the tip of the Drau–Möll Block coincides approximately with the boundary between cooling domains 1 and 2 of the ETD (Fig. 5a). Shortening in front of the Drau–Möll Block was greatest in the vicinity of this tip, i.e. in the Sonnblick Subdome (Fig. 6b), where the ages in this study indicate that rapid cooling of the ETD initiated as early as 30–25 Ma. Continued indentation by the Drau–Möll Block accommodated by dextral and sinistral motions of the conjugate MF and ZWF, respectively, effected further shortening of the ETD in the Hochalm Dome and extensional exhumation in the footwall of the KNF beginning no later than 23 Ma (Scharf et al., 2013a). Final indentation of the Drau–Möll Block induced eastward extrusion and rollback of the KNF relative to the tip of this block, such that exhumation migrated laterally into what then became cooling domain 3 of the EDT. Rapid cooling ended at 17 Ma according to fission track cooling ages (Fig. 6c, see discussion in Scharf et al., 2013a).

Northward indentation of the Southern Alps is also documented along the Giudicarie Belt along the western edge of the Southern Alps indenter (Pomella et al., 2011; 2012): Initial sinistral transpressive motion along this belt and the transpressive Meran–Mauls Fault resulted in incipient bending of the Periadriatic Fault beginning in late Oligocene time. This incipient indentation did not trigger much exhumation of the Tauern Window, but appears to have induced late Oligocene sinistral shearing in the core of the WTD (Schneider et al., 2013) as well as the aforementioned early exhumation of the eastern ETD at 30–25 Ma (Reddy et al., 1993; this study). However, most of the approximately 77 km of sinistral displacement along the Giudicarie Belt occurred in Miocene time (23–7 Ma, Scharf et al., 2013a; Schmid et al., 2013; Handy et al., 2015; Schneider et al., submitted for publication) and triggered rapid exhumation and cooling of the WTD (Fügenschuh et al., 1997).

7. Conclusions

The cooling pattern in the Tauern Window is related to the fragmentation of an initially triangular zone of little or no ductile deformation comprising mostly Austroalpine units in front of the Adriatic indenter (Fig. 6). With progressive indentation, this zone was subdivided into two, semi-rigid crustal blocks (Rieserferner and Drau–Möll blocks) along the leading edge of this indenter. Miocene doming, exhumation and cooling of the eastern part of the Tauern Window (ETD in Fig. 1) occurred directly in front of the Drau–Möll Block. A new $^{147}Sm/^{144}Nd$ isochron age of 25.7 ± 0.9 Ma on garnet that overgrows the main foliation in the ETD (Fig. 3) marks the age of Barrow-type, amphibolite-facies metamorphism (Tauernkristallisation) in the eastern part of the Tauern Window. This metamorphism overlapped with the onset of doming and orogen-parallel extensional shearing. The new $^{87}Rb/^{87}Sr$ white mica and biotite ages presented in this paper point to broadly coeval cooling of the Sonnblick and Hochalm subdomes within the ETD (Fig. 2) to below 500 and 300 °C at about 30–21 and 23–15 Ma, respectively (Fig. 5). The cooling ages of these mica systems decrease from the center of the Tauern Window towards the KNF, reaching 24–21 Ma ($^{87}Rb/^{87}Sr$ white mica) and 18–15 Ma ($^{87}Rb/^{87}Sr$ biotite) in the KNF footwall (Fig. 5). Taken together, the new and existing thermochronological data show that the ETD was folded and exhumed as a single unit; doming migrated perpendicular to the indentation direction and parallel to motion of the eastward rolling footwall of the KNF during lateral orogenic escape.

The relative age of doming and Tauernkristallisation differs within the Tauern Window; in the center they are broadly coeval, whereas towards the eastern and western margins, doming was coeval with orogen-parallel extensional shearing and clearly post-dated the Tauernkristallisation. This change in the relative age of doming and peak-thermal metamorphism reflects the migration of tectonic and erosional unroofing from the center to the ends of the Tauern Window during lateral orogenic escape in latest Oligocene and Miocene time.

Regarded on the scale of the orogen, the anomalous indentation and exhumation patterns in front of the Adriatic indenter appear to have formed during a Neogene switch in subduction polarity, from south-directed European subduction to north-directed Adriatic subduction beneath the Eastern Alps (Lippitsch et al., 2003; Schmid et al., 2004; Handy et al., 2015). This polarity switch drove cold wedges of Austroalpine crust, which had previously formed the upper plate of the European subduction, into the warm and weak orogenic edifice of previously accreted European crust.

Acknowledgments

Special thanks go to our Berlin colleagues, Audrey Bertrand, Susanne Schneider, Stefan Schmid (now in Zürich) and Claudio Rosenberg (now in Paris), as well as Manfred Rockenschaub and Manfred Linner from the Geological Survey of Austria for many helpful discussions. We also thank Stanislaw Grabala from the Geological Survey of Austria for the mechanical preparation of the samples and Monika Horschinegg from the Department of Lithospheric Research, Vienna, Austria, for her help with the isotopic analyses. This study was supported partly by the German Science Foundation (0424021104, DFG-project Ha 2403/10) in the form of a doctoral stipend to the first author, and partly by the unemployment fund of the German government. We greatly acknowledge the critical and helpful reviews of M. Calderon and anonymous reviewer. Finally, we appreciated the friendly assistance of Kathrin Aichorn and her team at the BIOS Center, Nationalpark Hohe Tauern in Austria in obtaining permission to work in protected wildlife areas.

Appendix A

Table 1A
Authors list, sample names, ages and T_c values used for the cooling pattern in Fig. 5.

Method	Sonnblick Subdome West (Core)		Sonnblick SubdomeCenter (Mallnitz)		Sonnblick SubdomeEast (Lamellae)	
	Ages/err	Sample Nr Author	Ages/err	Sample Nr Author	Ages/err	Sample Nr Author
Rb/Sr Wm 550 ± 50 °C Purdy and Jäger, 1976 Von Blanckenburg et al. 1989	26.9 ± 0.5 28.3 ± 0.8 26.9 ± 0.4 26.2 ± 0.4 30,0 ± 1.1 25.8 ± 0.5 34.7 ± 0.5	323/87 Reddy et al., 1993 86/87 Reddy et al., 1993 84/88 Reddy et al., 1993 87/88 Reddy et al., 1993 79/88 Reddy et al., 1993 46/86 Reddy et al. 1993 83/88 Reddy et al. 1993	27.1 ± 0.4 23.9 ± 0.5 25.5 ± 2.9	128/86 Reddy et al., 1993 224/86 Reddy et al., 1993 TF04-1b Glodny et al., 2008	20.7 ± 2.3 Deformation	TF04-5 Glodny et al., 2008 not used
Mean	28.1 ± 0.5		25.7 ± 0.6			
530 ± 40 °C Ar/Ar Hbl Harrison(1981) $^{147}Sm/^{144}Nd$ Grt formation						
420 °C K/Ar Wm Robbins (1972)	27.5 ± 1.0	3056 Lambert, 1970	21.0 ± 0.5 21.0 ± 1	CVI Oxburgh et al., 1966 C315 Oxburgh et al., 1966		
Mean	27.5 ± 1.0		21.0 ± 0.7			
Rb/Sr Bt 320 ± 40 °C K/Ar Bt 320 ± 40 °C Harrison et al. (1985) Del Moro et al. (1982) Jäger et al. (1967)	21.7 ± 0.1 20.5 ± 0.2 22.4 ± 0.2 22.9 ± 0.3 21.1 ± 0.2 20.3 ± 0.1 21.1 ± 0.1 22.3 ± 0.2 20.2 ± 0.1 20.8 ± 0.1 21.5 ± 0.1 21.3 ± 0.1 26.7 Exc. Ar	86/87 Reddy et al., 1993 80/88 Reddy et al., 1993 41/86 Reddy et al., 1993 40/86 Reddy et al., 1993 84/88 Reddy et al., 1993 87/88 Reddy et al., 1993 81/88 Reddy et al., 1993 323/87 Reddy et al., 1993 79/88 Reddy et al., 1993 46/86 Reddy et al., 1993 28/88 Reddy et al., 1993 83/88 Reddy et al. 1993 Lambert, 1970 not used	21.0 ± 0.2 19.1 ± 0.2 19.2 ± 0.3 20.6 ± 0.1	11R40 this study 224/86 Reddy et al., 1993 128/86 Reddy et al., 1993 82/86 Reddy et al., 1993	17.3 ± 0.2	11R31 this study
Mean	21.2 ± 0.1		20.2 ± 0.2		17.3 ± 0.2	
FTZ 240 ± 20 °C 2sigma Yamada et al., 1995	21.5 ± 1.4 18.0 ± 1.6 17.5 ± 2.0 17.5 1.6	115 Dunkl et al., 2003 116 Dunkl et al., 2003 164 Dunkl et al., 2003 126 Dunkl et al., 2003				
Mean ZHE 2sigma 190 ± 10 °C Wolf et al., 1996	18.8 ± 1.6 15.4 ± 2.8 15.6 ± 3.4 16.1 ± 1.2 19.1 ± 0.2 15.8 ± 6.4	TW51 Wölfler et al., 2012 TW111 Wölfler et al., 2012 TW110 Wölfler et al., 2012 TW44 Wölfler et al., 2012 TW108 Wölfler et al., 2012				
Mean	18.3 ± 0.8					

Table 1A *(continued)*

Method	Hochalm Subdome West (Gastein)		Hochalm Subdome Center (Mallnitz)		Hochalm SubdomeEast (Core)		Hochalm Subdome East (Rim)	
	Ages/err	Sample Nr Author	Ages/err	Sample Nr Author	Ages/err	Sample Nr Author	Ages/err	Sample Nr Author
Rb/Sr Wm 550 ± 50 °C Purdy and Jäger, 1976 Von Blanckenburg et al. 1989	24.7 ± 0.4	53961 Inger and Cliff, 1994			21.8 ± 0.5	G2038 Cliff et al., 1985	24.4 ± 0.3	182/1/2005 this study
	28.3 ± 1.4	53940 Inger and Cliff, 1994			22.6 ± 0.6	G3500 Cliff et al., 1985	21.1 ± 0.2	04R64 this study
	32.0 ± 1.0	53941 Inger and Cliff, 1994			27.0 ± 2.0	M504 Cliff et al., 1985	21.2 ± 1.0	H2000 Cliff et al., 1985
	28.4 ± 1.2	53942 Inger and Cliff, 1994			20.5 ± 1.2	M1480 Cliff et al., 1985	23.1 ± 0.6	H3000 Cliff et al., 1985
	29.0 ± 1.0	53943 Inger and Cliff, 1994			22.0 ± 2.0	M2085 Cliff et al., 1985	22.6 ± 0.6	H1000 Cliff et al., 1985
	26.2 ± 0.8	53944 Inger and Cliff, 1994					23.8 ± 0.4	G419 Cliff et al., 1985
	31.0 ± 2.0	53945 Inger and Cliff, 1994					22.3 ± 0.8	54037 Inger and Cliff, 1994
	23.3 ± 1.2	53948 Inger and Cliff, 1994					24.0 ± 2.5	53957 Inger and Cliff, 1994
	25.0 ± 1.7	53949 Inger and Cliff, 1994						
Mean	27.0 ± 1.0				22.3 ± 0.9		22.7 ± 0.5	
530 ± 40 °C Ar/Ar Hbl Harrison(1981) $^{147}Sm/^{144}Nd$ Grt formation	25.7 ± 0.9	155/6/2011 this study Sm/Nd Grt	23.8 ± 0.8	803a Cliff et al., 1985 Ar/Ar Hbl				
			24.0 ± 1.0	803a Cliff et al., 1985				
			25.0 ± 1.3	803a Cliff et al., 1985				
	25.7 ± 0.9		24.0 ± 1.0					
420 °C K/Ar Wm Robbins (1972)			17.5 ± 0.5	C31 Oxburgh et al., 1966	18.5 ± 0.5	M504 Roddick et al., 1980	25 no Err	H1000 Cliff et al., 1985
			21.0 ± 0.5	OVI Oxburgh et al., 1966	18.0 ± 0.5	M1480 Roddick et al., 1980	22.4 no Err	H2000 Cliff et al., 1985
			21.0 ± 1.0	C315 Oxburgh et al., 1966	22.2 ± 0.5	G3500 Cliff et al., 1985	24 no Err	H3000 Cliff et al., 1985
			25.5 ± 1.0	2280 Oxburgh et al., 1966	20.9 ± 0.5	Tr Cliff et al., 1971	21.5 ± 1.0	C495 Oxburgh et al., 1966
							23.5 ± 0.5	Gr Cliff et al., 1971
							27.9 Exc. Ar	G419 Cliff et al., 1985 not used
							22.0 ± 1.0	C422 Oxburgh et al., 1966
							22 ± 0.5	C55 Oxburgh et al., 1966
Mean			20.6 ± 0.7		19.9 ± 0.5		22.4 ± 0.7	
Rb/Sr Bt 320 ± 40 °C K/Ar Bt 320 ± 40 °C Harrison et al. (1985) Del Moro et al. (1982) Jäger et al. (1967)	20.6 ± 0.2	SF08-11 this study	20.5 ± 0.2	11R34 this study	16.3 ± 0.2	G2085 Cliff et al., 1985	18.1 ± 0.2	04R64 this study
	21.5 ± 0.5	2093 Oxburgh et al., 1966	19.0 ± 0.2	11R29 this study	16.5 ± 0.2	G2038 Cliff et al., 1985	17.9 ± 0.2	04R29 this study
			17.7 ± 0.2	11R35 this study	15.1 ± 0.2	G3500 Cliff et al., 1985	17.4 ± 0.2	182/1/2005 this study
			19.8 ± 0.2	155/2/2011 this study	16.5 ± 0.2	G4500 Cliff et al., 1985	18.6 ± 0.2	11R30 this study
			18.2 ± 0.2	181/1/2011 this study	16.2 ± 0.2	G5500 Cliff et al., 1985	15.3 ± 0.2	H3000 Cliff et al., 1985
			17.7 ± 0.2	11R46 this study	16.7 ± 0.4	M504 Cliff et al., 1985	16.1 ± 0.2	G419 Cliff et al., 1985
			17.5 ± 0.2	11R52 this study	17.2 ± 1.3	M990 Cliff et al., 1985	17.0 ± 0.3	H1000 Cliff et al., 1985
			19.5 ± 0.2	11R32 this study	16.4 ± 0.3	M1480 Cliff et al., 1985	19.5 ± 1.0	C18 Oxburgh et al., 1966
			18.0 ± 1.0	2279 Oxburgh et al., 1966	16.7 ± 0.2	C6716 Cliff and Cohen, 1980	22.0 ± 0.5 Exc. Ar	C213 Oxburgh et al., 1966 not used
			19.5 ± 0.5	C212 Oxburgh et al., 1966	21.9 ± 0.5	Z162 Cliff et al., 1971	19.0 ± 0.5	Gr Cliff et al., 1971
					21.5 ± 0.4	Z160 Cliff et al., 1971		
					16.0 ± 0.3	Z159 Cliff et al., 1971		
					16.1 ± 0.2	Z151 Cliff et al., 1971		
					17.5 ± 0.2	Z150 Cliff et al., 1971		
					25.2 ± 0.5 Exc. Ar	Tr Cliff et al., 1971: not used		
Mean	20.9 ± 0.3		18.8 ± 0.2		16.8 ± 0.3		17.7 ± 0.2	
FTZ 240 ± 20 °C 2sigma Yamada et al., 1995	18.4 ± 3.0	130 Dunkl et al., 2003	17.5 ± 2.0	128 Dunkl et al., 2003	11.8 ± 3.2	Bertrand, 2013	17.5 ± 1.4	KR-8 Dunkl et al., 2003
			18.5 ± 2.4	125 Dunkl et al., 2003	16.9 ± 1.6	113 Dunkl et al., 2003	17.1 ± 2.6	7–22 Dunkl et al., 2003
							16.7 ± 2.0	7–23 Dunkl et al., 2003
							10.4 ± 4.2	Bertrand, 2013
Mean	18.4 ± 3.0		18.0 ± 2.2		15.2 ± 2.0		16.5 ± 2.2	
ZHE 2sigma 190 ± 10 °C Wolf et al., 1996								
Mean								

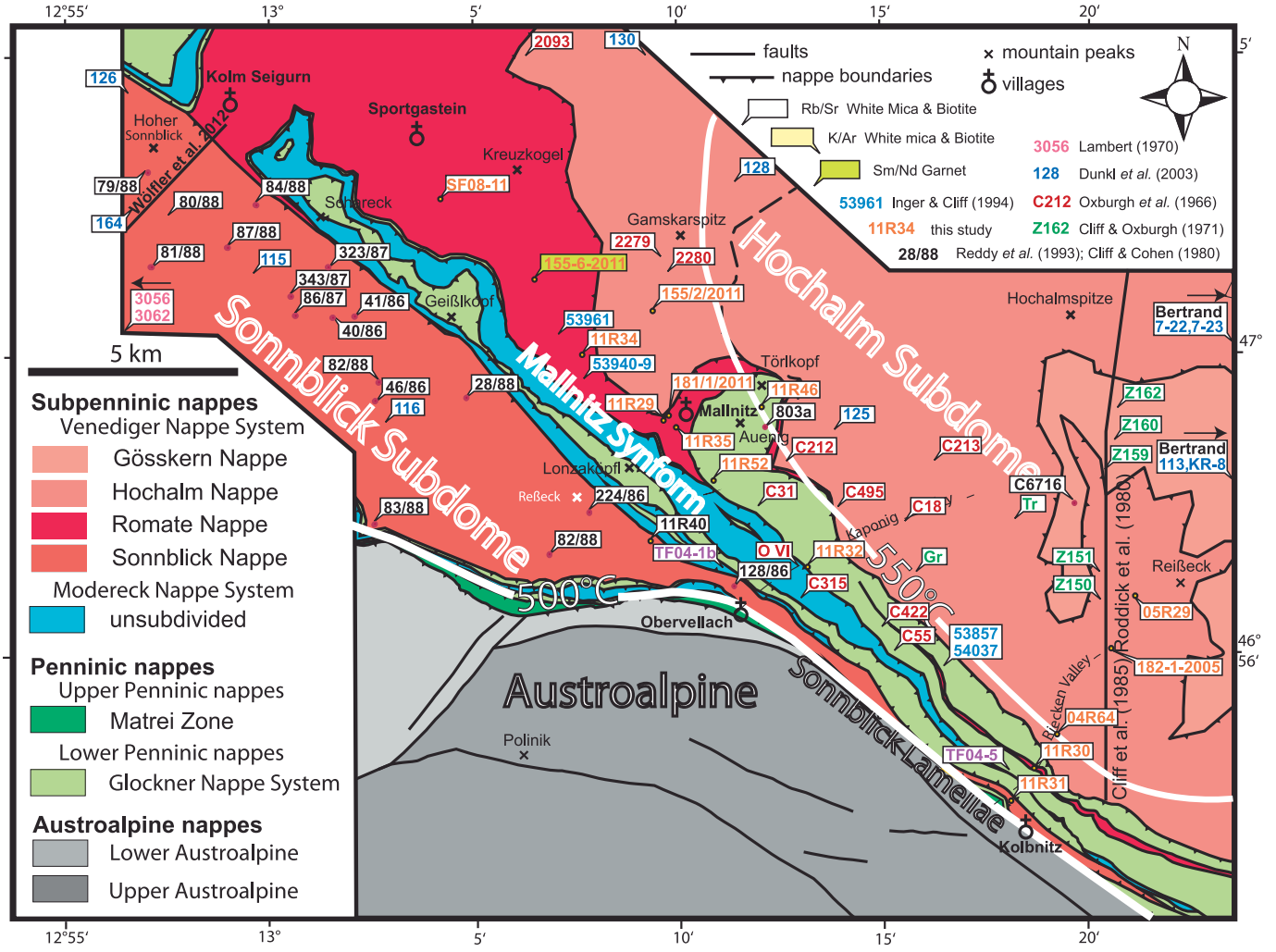

Fig. 1A. Sample map. Samples listed in Table 1 of the Appendix A.

References

Barnes, J.D., Selverstone, J., Sharp, Z.D., 2004. Interactions between serpentinite devolatilization, metasomatism and strike-slip strain localization during deep-crustal shearing in the Eastern Alps. J. Metamorph. Geol. 22, 283–300.

Becker, B., 1993. The structural evolution of the Radstadt Thrust System, Eastern Alps, Austria — kinematics, thrust geometries, strain analysis. Tübinger Geowissenschaftliche Arbeiten 14, 92.

Behrmann, H., 1988. Crustal-scale extension in a convergent orogen: the Sterzing–Steinach mylonite zone in the Eastern Alps. Geodin. Acta 2 (2), 63–73.

Bertrand, A., 2013. Exhuming the Core of Collisional Orogens, the Tauern Window (Eastern-Alps) A Geochronological, Modelling and Structural study (PhD thesis) Freie Universität Berlin, Berlin, Germany, p. 196.

Borsi, S., Del Moro, A., Sassi, F.P., Zirpoli, G., 1973. Metamorphic evolution of the Austric rocks to the south of the Tauern Window (eastern Alps): radiometric and geopetrologic data. Mem. Soc. Geol. Ital. 12, 549–571.

Borsi, S., Del Moro, A., Sassi, F.P., Zanferrari, A., Zirpoli, G., 1978. New geopetrologic and radiometric data on the Alpine history of the Austridic continental margin south of the Tauern Window (Eastern Alps). Memorie degli Instituti di Geologia e Mineralogia dell'Università di Padova. 32 pp. 1–17.

Bousquet, R., Oberhänsli, R., Schmid, S.M., Berger, A., Wiederkehr, M., Robert, C., Möller, A., Rosenberg, C., Zeilinger, G., Molli, G., Koller, F., 2012. Metamorphic framework of the Alps. Commission for the Geological Map of the World (CCGM/CGMW).

Cliff, R.A., Cohen, A., 1980. Uranium–lead isotope systematics in a regionally metamorphosed tonalite from the Eastern Alps. Earth Planet. Sci. Lett. 50, 211–218.

Cliff, R.A., Norris, R.J., Oxburgh, E.R., Wright, R.C., 1971. Structural, metamorphic and geochronological studies in the Reisseck and southern Ankogel Groups, the Eastern Alps. Jahrbuch der Geologischen Bundesanstalt Wien 144 (2), 121–279.

Cliff, R.A., Droop, G.T.R., Rex, D.C., 1985. Alpine metamorphism in the south-east Tauern Window, Austria: 2. Rates of heating, cooling and uplift. J. Metamorph. Geol. 3, 403–415.

Cliff, R.A., Oberli, O., Droop, G.T.R., 1998. Achieving geological precision in metamorphic geochronology: a Th–Pb age for the syn-metamorphic formation of the Mallnitzermulde Synform, Tauern Window, from individual allanite porphyroblasts. J. Conf. Abstr. V.M. Goldschmidt Conf. 62A, 337–338.

Dachs, E., Kurz, W., Proyer, A., 2005. Alpine eclogites in the Tauern Window. Mitt. Österr. Mineralogischen Ges. 150, 199–226.

Dal Piaz, G.V., 1999. The Austroalpine–Piedmont nappe stack and the puzzle of Alpine Tethys. Mem. Sci. Geol. 51 (1), 155–176.

Del Moro, A., Puxeddu, M., Radicati di Brozolo, F., Villa, I.M., 1982. Rb/Sr and K–Ar ages on minerals at temperatures of 300°–400 ° C from deep wells in the Larderello geothermal field (Italy). Contrib. Mineral. Petrol. 81 (4), 340–349.

Droop, G.T.R., 1985. Alpine metamorphism in the south-east Tauern Window, Austria: 1. P–T variations in space and time. J. Metamorph. Geol. 3, 371–402.

Droop, G.T.R., 2013. Paragonite in marbles from the Tauern Window, Austria: compositional and thermobaric controls. Lithos 162–163, 1–13.

Dunkl, I., Frisch, W., Grundmann, G., 2003. Zircon fission track thermochronology of the southeastern part of the Tauern Window and adjacent Austroalpine margin, Eastern Alps. Eclogae Geol. Helv. 96, 209–217.

England, P.C., Thompson, A.B., 1984. Pressure–temperature–time paths of regional metamorphism I. Heat transfer during the evolution of regions of thickened continental crust. J. Petrol. 25, 894–928.

Exner, C., 1962. Geologische Karte der Sonnblickgruppe, M 1:50000. *Geologische Bundesanstalt Wien, Wien.*

Exner, C., 1964. Erläuterungen zur Geologischen Karte der Sonnblickgruppe. Geologische Bundesanstalt Wien, Wien 1:50000.

Exner, C., 1971. Geologie der peripheren Hafnergruppe (Hohe Tauern). Jahrbuch der Geologischen Bundesanstalt, Wien 114, 1–119.

Exner, C., 1982. Geologie der zentralen Hafnergruppe (Hohe Tauern). Jahrbuch der Geologischen Bundesanstalt, Wien 125 (1–2), 51–154.

Exner, C., 1984. Der Südrand des Tauernfensters bei Spittal an der Drau. Jahrbuch der Geologischen Bundesanstalt, Wien 127 (3), 349–367.

Favaro, S., Schuster, R., 2012. Bericht 2012 über geologische Aufnahmen auf den Blättern 154 Rauris, 155 Bad Hofgastein und 181 Obervellach. Jahrbuch der Geologischen Bundesanstalt Wien 152 (1–4), 268–272.

Feitzinger, G., Paar, W.H., 1991. Gangförmige Gold–Silber–Vererzungen in der Sonnblickgruppe (Hohe Tauern, Kärnten). Arch. Lagerstättenforsch. Geol. Bundesanst. 13, 17–50.

Fodor, L., Jelen, B., Márton, E., Skaberne, D., Čar, J., Vrabec, M., 1998. Miocene–Pliocene tectonic evolution of the Slovenian Periadriatic fault: implications for Alpine–Carpathian extrusion models. Tectonics 17 (5), 690–709.

Foeken, J.P.T., Persano, C., Stuart, F.M., ter Voorde, M., 2007. Role of topography in isotherm perturbation: apatite (U–Th)/He and fission track results from the Malta tunnel, Tauern Window, Austria. Tectonics 26. http://dx.doi.org/10.10129/2006TC002049.

Frisch, W., Kuhlemann, J., Dunkl, I., Brügel, A., 1998. Palinspastic reconstruction and topographic evolution of the Eastern Alps during late Cenozoic tectonic extrusion. Tectonophysics 297, 1–15.

Frisch, W., Dunkl, I., Kuhlemann, J., 2000. Post-collisional orogen-parallel large-scale extension in the Eastern Alps. Tectonophysics 327, 239–265.

Fügenschuh, B., Seward, D., Mantckelow, N.S., 1997. Exhumation in a convergent orogen: the western Tauern Window. Terra Nova 9, 213–217.

Genser, J., Neubauer, F., 1989. Low angle normal faults at the eastern margin of the Tauern window (Eastern Alps). Mitt. Österr. Geol. Ges. 81, 233–243.

Genser, J., van Wees, J.D., Cloething, S., Neubauer, F., 1996. Eastern Alpine tectonometamorphic evolution: constraints from two-dimensional P–T–t modeling. Tectonics 15, 584–604.

Gipper, P., 2012. Crustal Imbrication and Nappe Folding in the southeastern Tauern Window (Master thesis) Freie Universität Berlin, Berlin, Germany.

Glodny, J., Ring, U., Kühn, A., Gleissner, P., Franz, G., 2005. Crystallization and very rapid exhumation of the youngest Alpine eclogites (Tauern Window, Eastern Alps) from $^{87}Rb/^{86}Sr$ mineral assemblage analysis. Contrib. Mineral. Petrol. 149, 699–712.

Glodny, J., Ring, U., Kühn, A., 2008. Coeval high-pressure metamorphism, thrusting, strike-slip, and extensional shearing in the Tauern Window, Eastern Alps. Tectonics 27, TC4004. http://dx.doi.org/10.1029/2007TC002193.

Handy, M.R., Babist, J., Rosenberg, C.L., Wagner, R., Konrad, M., 2005. Decoupling and is relation to strain partitioning in continental lithosphere — insight from the Periadriatic fault system (European Alps). In: Gapais, D., Brun, J.P., Cobbold, P.R. (Eds.), Deformation Mechanism, Rheology and Tectonics. Geological Society of London, Special Publication 243, pp. 249–276.

Handy, M.R., Schmid, S.M., Bousquet, R., Kissling, E., Bernoulli, D., 2010. Reconciling plate-tectonic reconstructions of Alpine Tethys with the geological–geophysical record of spreading and subduction in the Alps. Earth Sci. Rev. 102, 121–158. http://dx.doi.org/10.1016/j.earscirev.2010.06.002.

Handy, M.R., Ustaszewsky, K., Kissling, E., 2015. Reconstructing the Alps–Carpathians–Dinarides as a key to understanding switches in subduction polarity, slab gaps and surface motion. Int. J. Earth Sci. 104 (1), 1–26. http://dx.doi.org/10.1007/s00531-014-1060-3.

Harrison, T.M., 1981. Diffusion of ^{40}Ar in hornblende. Contrib. Mineral. Petrol. 78, 324–331.

Harrison, T.M., Duncan, I., McDougall, I., 1985. Diffusion of ^{40}Ar in biotite: temperature, pressure and compositional effects. Geochim. Cosmochim. Acta 49, 2461–2468.

Hawemann, F., 2013. Metamorphic Conditions During Crustal Imbrication and Nappe Stacking in the Southeastern Tauern Window (Master thesis) Freie Universität Berlin, Berlin, Germany.

Hoinkes, G., Koller, F., Rantitsch, G., Dachs, E., Hock, V., Neubauer, F., Schuster, R., 1999. Alpine metamorphism of the Eastern Alps. Schweiz. Mineral. Petrogr. Mitt. 79, 155–181.

Hoke, L., 1990. The Altkristallin of the Kreuzeck Mountains, SE Tauern Window, Eastern Alps-basement crust in a convergent plate boundary zone. Jahrbuch der Geologischen Bundesanstalt, Wien 133, 5–87.

Horvath, F., Bada, G., Szafián, P., Tari, G., Ádám, A., Cloetingh, S., 2006. Formation and deformation of the Pannonian basin: constraints from observational data. In: Gee, D.G., Stephenson, R.A. (Eds.), European Lithosphere Dynamics, Memoirs, Geological Society of London 32, pp. 191–206.

Inger, S., Cliff, R.A., 1994. Timing of metamorphism in the Tauern Window, Eastern Alps: Rb/Sr ages and fabric formation. J. Metamorph. Geol. 12, 695–707.

Jäger, E., Niggli, E., Wenk, E., 1967. Rb/Sr Attersbestimmungen an Glimmern der Zentralalpen. Beiträge zur geologische Karte der Schweiz, NF 1344, Bern: 67.

Kober, L., 1920. Das Östliche Tauernfenster. *Denkschrift der Akademie der Wissenschaften Wien*, Mathematisch-Naturwissenschaftliche Klasse, Abt I, 98pp. 201–243.

Kurz, W., Neubauer, F., 1996. Deformation partitioning during updoming of the Sonnblick area in the Tauern Window (Eastern Alps, Austria). J. Struct. Geol. 18 (11), 1327–1343.

Kurz, W., Neubauer, F., Genser, J., 1996. Kinematics of Penninic nappes (Glockner Nappe and basement-cover nappes) in the Tauern Window (Eastern Alps, Austria) during subduction and Penninic–Austroalpine collision. Eclogae Geol. Helv. 89 (1), 573–605.

Kurz, W., Neubauer, F., Dachs, E., 1998. Eclogite meso- and microfabrics: implications for the burial and exhumation history of eclogites in the Tauern Window (Eastern Alps) from P–T–d paths. Tectonophysics 285, 183–209.

Kurz, W., Handler, R., Bertoldi, C., 2008. Tracing the exhumation of the Eclogite Zone (Tauern Window, Eastern Alps) by $^{40}Ar/^{39}Ar$ dating of white mica in eclogites. Swiss J. Geosci. 101 (1), 191–S206.

Lambert, R.S.t.J., 1970. A potassium–argon study of the margin of the Tauernfenster at Döllach, Austria. Eclogae Geol. Helv. 63, 197–205.

Läufer, A.L., Frisch, W., Steinitz, G., Loeschke, J., 1997. Exhumed fault-bounded blocks along the Periadriatic lineament. Geol. Rundsch. 86, 612–626.

Linner, M., Reitner, J.M. and Pavlik, W., 2013. Geologische Karte der Republik Österreich 1: 50000 Blatt 179 Lienz. Geologische Bundesanstalt, Wien.

Linzer, H.G., Decker, K., Peresson, H., Dell'Mour, R., Frisch, W., 2002. Balancing lateral orogenic float of the Eastern Alps. Tectonophysics 54, 211–237.

Lippitsch, R., Kissling, E., Ansorge, J., 2003. Upper mantle structure beneath the Alpine orogen from high-resolution teleseismic tomography. J. Geophys. Res. 108 (B8), 2376. http://dx.doi.org/10.1029/2002JB002016.

Ludwig, K.R., 2001. Isoplot/Ex version 2.49. A Geochronological toolkit for Microsoft Excel. Berkeley Geochronology Center Special Publicationp. 1a.

Ludwig, K.R., 2003. Isoplot/Ex version 3.0. A geochronological toolkit for Microsoft Excel. Berkeley Geochronological Centre Special Publication (70 p.).

Luth, S.W., Willingshofer, E., 2008. Mapping of the post-collisional cooling history of the Eastern Alps. Swiss J. Geosci. 101, 207–223.

Luth, S., Willingshofer, E., ter Borgh, M., Sokoutis, D., van Otterloo, J., Versteeg, A., 2013. Kinematic analysis and analogue modeling of the Passeier- and Jaufen faults: implications for crustal indentation in the Eastern Alps. Int. J. Earth Sci. 102, 1071–1090. http://dx.doi.org/10.1007/s00531-012-0846-4.

Mancktelow, N.S., Stöckli, D.F., Grollimund, B., Müller, W., Fügenschuh, B., Viola, G., Seward, D., Villa, I.M., 2001. The DAV and Periadriatic fault systems in the Eastern Alps south of the Tauern window. Int. J. Earth Sci. 90, 593–622.

McCullogh, M.T., Wasserburg, G.J., 1978. Sm–Nd and Rb/Sr chronology of continental crust formation. Science 200, 1003–1011.

Means, W.D., 1989. Stretching faults. Geology 17, 893–896.

Müller, W., 1998. Isotopic dating of deformation using microsampling techniques: the evolution of the Periadriatic Fault System (Alps) (Ph.D. thesis), ETH Zürich (135 p.).

Müller, W., Mancktelow, N.S., Meier, M., 2000. Rb–Sr microchrones of synkinematic mica in mylonites: an example from the DAV fault of the Eastern Alps. Earth Planet. Sci. Lett. 180, 385–397.

Müller, W., Prosser, G., Mancktelow, N.S., Villa, I.M., Kelley, S.P., Viola, G., Oberli, F., 2001. Geochronological constraints on the evolution of the Periadriatic Fault System (Alps). Int. J. Earth Sci. 90, 623–653.

Nagel, T.J., Herwartz, D., Rexroth, S., Münker, C., Froitzheim, N., Kurz, W., 2013. Lu–Hf dating, petrography, and tectonic implications of the youngest Alpine eclogites (Tauern Window, Austria). Lithos 170 (171), 179–190.

Oxburgh, E.R., Lambert, R.S.t.J., Baadsgaard, H., Simons, J.G., 1966. Potassium–argon age studies across the southeast margin of the Tauern Window, the Eastern Alps. Verhandlungen der Geologischen Bundesanstalt, Wien 17–33.

Pestal, G., Hellerschmidt-Alber, J., 2011. Bericht 2009 und 2010 über geologische Aufnahmen auf Blatt 154 Rauris. Jahrbuch der Geologischen Bundesanstalt, Wien 151 (1–2), 142–148.

Pestal, G., Hejl, E., Braunstingl, R. and Schuster, R., 2009. Erläuterungen Geologische Karte von Salzburg 1 : 200.000. *Land Salzburg und Geologische Bundesanstalt Wien*, 1–162.

Pollington, A.D., Baxter, E., 2010. High resolution Sm–Nd garnet geochronology reveals the uneven pace of tectonometamorphic processes. Earth Planet. Sci. Lett. 293, 63–71.

Pomella, H., Klötzli, U., Scholger, R., Stipp, M., Fügenschuh, B., 2011. The Northern Giudicarie and the Meran–Mauls fault (Alps, Northern Italy) in the light of new paleomagnetic and geochronological data from boudinaged Eo-/Oligocene tonalites. Int. J. Earth Sci. 100, 1827–1850. http://dx.doi.org/10.1007/s00531-010-0612-4.

Pomella, H., Stipp, M., Fügenschuh, B., 2012. Thermochronological record of thrusting and strike-slip faulting along the Giudicarie fault system (Alps, Northern Italy). Tectonophysics 579, 118–130. http://dx.doi.org/10.1016/j.tecto.2012.04.015.

Purdy, J.W., Jäger, E., 1976. K–Ar ages on rock-forming minerals from the Central Alps. Memorie degli Istituti di Geologia e Mineralogia dell'Università de Padova. 30.

Raith, M., Raase, P., Kreuzer, H., Moller, 1978. The age of the Alpidic metamorphism in the Western Tauern Window, Austrian Alps, according to radiometric dating. In: Cless, H., Roeder, D., Schmid, K. (Eds.), Alps, Appenines and Hellenides, Inter-Union Commission on Geodynamics, Scientific Report No. 38, pp. 140–149.

Rantitsch, G., 2001. Thermal history of the Drau Range (Eastern Alps). Schweiz. Mineral. Petrogr. Mitt. 81, 181–196.

Ratschbacher, L., Frisch, W., Neubauer, F., Schmid, S.M., Neugebauer, J., 1989. Extension in compressional orogenic belts: the Eastern Alps. Geology 17, 404–407.

Ratschbacher, L., Merle, O., Davy, P., Cobbold, P., 1991a. Lateral extrusion in the eastern Alps, Part1: boundary conditions and experiments scaled for gravity. Tectonics 10, 245–256.

Ratschbacher, L., Frisch, W., Linzer, H.G., Merle, O., 1991b. Lateral extrusion in the Eastern Alps, Part2: structural analysis. Tectonics 10, 257–271.

Ratschbacher, L., Dingeldey, Ch., Miller, Ch., Hacker, B.R., McWilliams, M.O., 2004. Formation, subduction, and exhumation of Penninic oceanic crust in the Eastern Alps: time constraints from $^{40}Ar/^{39}Ar$ geochronology. Tectonophysics 394, 155–170.

Reddy, S.M., Cliff, R.A., East, R., 1993. Thermal history of the Sonnblick Subdome, southeast Tauern Window, Austria: implications for heterogeneous uplift within the Pennine Basement. Geol. Rundsch. 82, 667–675.

Robbins, G.A., 1972. Radiogenic Argon Diffusion in Muscovite Under Hydrothermal Conditions (M.Sc. Thesis) Brown University, Rhode Island.

Roddick, J.C., Cliff, R.A., Rex, D.C., 1980. The evolution of excess argon in Alpine biotite — a $^{39}Ar/^{40}Ar$ analysis. Earth Planet. Sci. Lett. 48, 185–208.

Romer, R.L., Siegesmund, S., 2003. Why allanite may swindle about its true age. Contrib. Mineral. Petrol. 146, 297–307.

Rosenberg, C.L., 2004. Shear zones and magma ascent: a model based on a review of the Tertiary magmatism in the Alps. Tectonics 23, 1–21.

Rosenberg, C.L., Schneider, S., 2008. The western termination of the SEMP Fault (eastern Alps) and is bearing on the exhumation of the Tauern Window. Geol. Soc. Lond. Spec. Publ. 298, 197–218.

Rosenberg, C.L., Brun, J.P., Cagnard, F., Gapais, D., 2007. Oblique indentation in the Eastern Alps: insights from laboratory experiments. Tectonics 26, TC2003. http://dx.doi.org/10.1029/2006TC 001960.

Royden, L.H., Burchfield, B.C., 1989. Are systematic variations in thrust belt style related to plate boundary processes? (The western Alps versus the Carparthians). Tectonics 8, 51–61.

Sander, B., 1911. Geologische Studien am Westende der hohen Tauern. Bericht—Denkschrift d. kais. Akademie der Wissenschaften, Wien 83, 257–319.

Satir, M., 1975. Die Entwicklungsgeschichte der westlichen Hohen Tauern und der südlichen Ötztalmasse auf Grund radiometrischer Altersbestimmungen (Ph.D. thesis) Società cooperativa tipografica, Padova, pp. 1–84.
Scharf, A., Handy, M.R., Favaro, S., Schmid, S.M., Bertrand, A., 2013a. Modes of orogen-parallel stretching and extensional exhumation of thickening orogenic crust in response to microplate indentation and slab roll-back (Tauern Window, Eastern Alps). Int. J. Earth Sci. 102 (6), 1627–1654. http://dx.doi.org/10.1007/s00531-013-0894-4.
Scharf, A., Handy, M.R., Ziemann, M.A., Schmid, S.M., 2013b. Peak-temperature patterns of polyphase metamorphism resulting from accretion, subduction and collision (eastern Tauern Window, European Alps) — a study with Raman microspectroscopy on carbonaceous material (RSCM). J. Metamorph. Geol. 31 (8), 863–880. http://dx.doi.org/10.1111/jmg.12048.
Scharf, A., Handy, M.R., Schmid, S.M., Favaro, S., Sudo, M., Schuster, R., Hammerschmidt, K., 2015. Grain-size effects on the closure temperature of white mica in a crustal-scale extensional shear zone — implications for dating shearing and cooling from in-situ $^{40}Ar/^{39}Ar$ laser-ablation ages of white mica (Tauern Window, Eastern Alps). Tectonophysics (submitted for publication).
Schmid, S.M., Fügenschuh, B., Kissling, E., Schuster, R., 2004. Tectonic map and overall architecture of the Alpine orogen. Eclogae Geol. Helv. 97, 93–117.
Schmid, S.M., Bernoulli, D., Fügenschuh, B., Matenco, L., Schefer, S., Schuster, R., Tischler, M., Ustaszewsky, K., 2008. The Alpine–Carpathian–Dinaridic system: correlation and evolution of tectonic units. Swiss J. Geosci. 101 (1), 139–183.
Schmid, S.M., Scharf, A., Handy, M.R., Rosenberg, C.L., 2013. The Tauern Window (Eastern Alps, Austria) — a new tectonic map, cross-sections and tectonometamorphic synthesis. Swiss J. Geosci. 106, 1–32. http://dx.doi.org/10.1007/s00015-013-0123-y.
Schneider, S., Hammerschmidt, K., Rosenberg, C.L., 2013. Dating the longevity of ductile shear zones: insight from $^{40}Ar/^{39}Ar$ in situ analyses. Earth Planet. Sci. Lett. 369–370, 43–58. http://dx.doi.org/10.1016/j.epsl.2013.03.002.
Schneider, S., Hammerschmidt, K., Rosenberg, C.L., Gerdes, A., Frei, D., Bertrand, A., 2015. U–Pb ages of apatite in the western Tauern Window (Eastern Alps): tracing the onset of collision-related exhumation in the European plate. Earth Planet. Sci. Lett. 418, 53–65. http://dx.doi.org/10.1016/j.epsl.2015.02.020.
Schneider, S., Rosenberg, C.L., Scharf, A., Hammerschmidt, K., 2015. Translation of indentation into lateral extrusion across a restraining bend: the western Tauern Window, Eastern Alps. Tectonics (submitted for publication).
Schuster, R., Koller, F., Hoeck, V., Hoinkes, G., Bousquet, R., 2004. Explanatory notes to the map: metamorphic structure of the Alps — metamorphic evolution of the Eastern Alps. Mitt. Österr. Mineralogischen Ges. 149, 175–199.
Schuster, R., Tropper, P., Krenn, E., Finger, F., Frank, W., Philippisch, R., 2015. Prograde Permo-Triassic metamorphic HT/LP assemblages from the Austroalpine Jenig Complex (Carinthia, Austria). Aust. J. Earth Sci. 108 (1), 73–90.
Selverstone, J., 1985. Petrologic constraints on imbrication, metamorphism, and uplift in the SW Tauern Window, Eastern Alps. Tectonics 4, 687–704.
Selverstone, J., 1988. Evidence for east–west crustal extension in the Eastern Alps: implications for the unroofing history of the Tauern Window. Tectonics 7, 87–105.
Selverstone, J., 2005. Are the Alps collapsing? Annu. Rev. Earth Planet. Sci. 33, 113–132.
Selverstone, J., Morteani, G., Staude, J.M., 1991. Fluid channeling during ductile shearing — transformation of granodiorite into aluminous schist in the Tauern Window, Eastern Alps. J. Metamorph. Geol. 9, 419–431.
Sölva, H., Grasemann, B., Thöni, M., Thiede, R., Habler, G., 2005. The Schneeberg Normal Fault Zone: normal faulting associated with Cretaceous SE-directed extrusion in the Eastern Alps (Italy/ Austria). Tectonophysics 401, 143–166.
Staub, R., 1924. Der Bau der Alpen. *Betrieb Geologische Karte Schweiz* (*N.F.*), 52, 272.
Staufenberg, H., 1987. Apatite fission-track evidence for postmetamorphic uplift and cooling history of the Eastern Tauern Window and the surrounding Austroalpine (Central Eastern Alps, Austria). Jahrbuch der Geologischen Bundesanstalt, Wien 130, 571–586.
Stipp, M., Stünitz, H., Heilbronner, R., Schmid, S.M., 2002. The eastern Tonale fault zone: a natural laboratory for crystal plastic deformation of quartz over a temperature range from 250 to 700 °C. J. Struct. Geol. 24, 1861–1884.
Stöckhert, B., Brix, M.R., Kleinschrodt, R., Huford, A.J., Wirth, R., 1999. Thermochronometry and microstructures of quartz—a comparison with experimental flow laws and predictions on the temperature of the brittle-plastic-transition. J. Struct. Geol. 21, 351–369.
Tapponnier, P., Peltzer, G., Armijo, R., 1986. On the mechanics of the collision between India and Asia. Geol. Soc. Lond. Spec. Publ. 19, 113–157.
Thiele, O., 1980. Das Tauernfenster. In: Oberhauser, R. (Ed.), *Der Geologische Aufbau Österreichs*, (300–314). Springer, Wien.
Thöni, M., 1980. Distribution of pre-Alpine and Alpine metamorphism of the southern Ötztal Mass and the Scarl Unit based on K/Ar age determinations. Mitteilungen der österreichischen geologischen Gesellschaft, Wien 71, 139–165.
Tollmann, A., 1977. Geologic von Oesterreich, I, Die Zentralalpen. Franz Deuticke, Vienna.
Trümpy, R., 1973. The timing of orogenic events in the Central Alps. In: De Jong, K.A., Scholten, R. (Eds.), Gravity and Tectonics. J. Wiley and Sons, pp. 229–251.
von Blanckenburg, F., Villa, I.M., Baur, H., Morteani, G., Steiger, R.H., 1989. Time calibration of a PT-path from the Western Tauern Window, Eastern Alps: the problem of closure temperatures. Contrib. Mineral. Petrol. 101, 1–11.
Wagner, R., Rosenberg, C.L., Handy, M.R., Möbus, C., Abertz, M., 2006. Fracture-driven intrusion and upwelling of a mid-crust pluton fed from a transpressive shear zone — the Rieserferner Pluton (Eastern Alps). Geol. Soc. Am. Bull. 118 (1–2), 219–237. http://dx.doi.org/10.1130/B25841.1.
Wolf, R.A., Farley, K.A., Silver, L.T., 1996. Helium diffusion and low temperature thermochronometry of apatite. Geochim. Cosmochim. Acta 60, 4231–4240.
Wölfler, A., Dekant, C., Danisík, M., Kurz, W., Dunkl, I., Putis, M., Frisch, W., 2008. Late stage differential exhumation of crustal blocks in the central Eastern Alps: evidence from fission track and (U–Th)/He thermochronology. Terra Nova 20, 378–384.
Wölfler, A., Stüwe, K., Danišik, M., Evans, N.J., 2012. Low temperature thermochronology in the Eastern Alps: implications for structural and topographic evolution. Tectonophysics 541–543, 1–18. http://dx.doi.org/10.1016/j.tecto.2012.03.016.
Wölfler, A., Dekant, Ch., Frisch, W., Danišik, M., Frank, W., 2015. Cretaceous to Miocene cooling of Austroalpine units southeast of the Tauern Window (Eastern Alps) constrained by multi-system thermochronometry. Aust. J. Earth Sci. 108 (1), 16–33.
Yamada, R., Tagami, T., Nishimura, S., Ito, H., 1995. Annealing kinetics of fission tracks in zircon; an experimental study. Chem. Geol. 122, 249–258.